AAPM REPORT NO. 71

A PRIMER FOR RADIOIMMUNOTHERAPY AND RADIONUCLIDE THERAPY

Report of Task Group #7
AAPM Nuclear Medicine Committee

Daniel J. Macey
Lawrence E. Williams (Chairman)
Hazel B. Breitz
An Liu
Timothy K. Johnson
Pat B. Zanzonico

April 2001

Published for the
American Association of Physicists in Medicine
by Medical Physics Publishing

Further copies of this report ($10 prepaid) may be obtained from:

Medical Physics Publishing
4513 Vernon Blvd.
Madison, WI 53705-4964
Telephone: 1-800-442-5778 or
608-262-4021
Fax: 608-265-2121
Email: mpp@medicalphysics.org
Web site: www.medicalphysics.org

International Standard Book Number: 1-888340-29-0
International Standard Serial Number: 0271-7344

Published by Medical Physics Publishing
4513 Vernon Blvd., Madison, WI 53705-4964

Printed in the United States of America

TABLE OF CONTENTS

LIST OF TABLES

LIST OF FIGURES

Terms for Internal Dosimetry

Term	Symbol	Traditional Units	SI Units
Administered radioactivity	A_0	μCi, mCi	MBq, GBq
Anterior counts	N_{ap}	number	number
Attenuation correction factor	ACF		
Biological half time	$T_{1/2b}$	h	h
Body thickness	T	cm	m
Cumulated activity	$\tilde{A}$	μCi-h	number
Effective half time	T_{eff}	h	h
Geometric mean count	GM	number	number
Organ or tumor thickness	ℓ	cm	m
Percent Injected Activity	PIA (not decay-corrected)		number
Percent Injected Dose	PID (decay-corrected)		number
Physical half time	$T_{1/2p}$	h	h
Posterior counts	N_{pa}	number	number
Remainder body	RB		
Residence time	τ	h	h
S values (target *t*, source *s*)	$S_{t \leftarrow s}$	rad/μCi-h	cGy/MBq-h
Sensitivity of Anger camera	ε	counts/μCi-s	counts/MBq-s
Total (Whole) Body	WB		

I. RADIONUCLIDE THERAPY PRINCIPLES

A. Objectives and Scope of the Primer

Recent trends in radionuclide therapy with radiolabeled antibodies and bone-seeking radiopharmaceuticals have promoted renewed interest in providing more accurate radiation absorbed dose estimates. A wide range of radionuclides (Table 1), attached to a variety of targeting agents, have been used in these trials. For many of the protocols, radiation absorbed dose estimates are relied on to decide whether a patient should proceed to therapy and for prescribing the amount of activity that should be administered. The motivation for this primer is the provision of absorbed dose estimates for individual patients within the limitations of the associated methodology. Although the MIRD Pamphlet 11 S values (Snyder et al. 1975) have been used to provide the framework for radiation absorbed dose estimates for patients undergoing diagnostic studies with radionuclides, more accurate methods are required for radionuclide therapy procedures. Here, the organ volumes and geometry of standard man models may not apply. More accurate dose estimates for each patient are also important for establishing fundamental dose-response relationships for toxicity and efficacy of Radioimmunotherapy (RIT).

This primer introduces various approaches to internal dose estimation in a therapeutic context. The methodology may also be applied to diagnostic dose estimates. The primer is intended for clinical physicists, radiation oncologists, nuclear medicine physicians, dosimetrists, nuclear medicine technologists, and other hospital personnel who are or will be involved in the process of acquiring and processing dose estimation data.

B. Dose Estimation Relationships

A fundamental equality generally assumed in the estimation of organ doses is the familiar equation:

$$D_{t\leftarrow s}[rad] = S_{t\leftarrow s}\left[\frac{rad}{\mu Ci - h}\right]\cdot \tilde{A}_s[\mu Ci - h] \tag{1}$$

where: $S_{t\leftarrow s}$ is a rectangular matrix giving the dose to a target organ t per unit time-activity in a source organ s (Loevinger and Berman 1976, Loevinger et al. 1991). Conceptually, eq. (1) separates the analytic process into two segments. Given the radionuclide, S refers purely to geometric factors. The cumulated activity $\tilde{A}_S$ is the area under the curve of activity (A_S) versus time. Traditional dimensions, rad/(μCi-h) for S, are changed to cGy/MBq-h for SI units. Notice that D and $\tilde{A}$ are

Table 1. A Partial List of Radionuclides Used in Internal Emitter Therapy

Radionuclide	Half Life	E_β max (MeV)	E_γ (MeV)
^{32}P	14.3 d	1.70	None
^{64}Cu	12.9 h	0.57 (β^-); 0.66 (β^+)	0.510 (38%)
^{67}Cu	61 h	0.57	0.180 (40%)
^{89}Sr	50.5 d	1.46	
^{90}Y	64.3 h	2.3	
^{117m}Sn	13.6 d	0.13; 0.16	0.158 (87%)
^{131}I	8.1 d	0.61	0.365 (81%)
^{153}Sm	1.9 d	0.81	0.103 (29%)
^{186}Re	3.8 d	1.07	0.137 (9%)
^{188}Re	17 h	2.12	0.16 (10%)
^{177}Lu	6.8 d	0.50	0.21 (6%)

Note: All beta emissions are for electrons except in the case of ^{64}Cu, which emits both electrons and positrons.

column vectors in this formula; their various elements refer to the source and target organs for a specified radionuclide. If one divides by the injected activity A_0, the resultant quantity is termed the residence time τ. Thus, dose per unit injected activity is the product of S and τ; this result is often used in reporting estimated doses. By changing the spatial perspective, elements of the S matrix may be made to represent other geometric positions such as voxels within an organ or tumor. In such cases the $\tilde{A}$ vector will represent integrated activities in organ voxels. A short glossary of terms used in internal emitter absorbed dose estimation is included at the front of this document.

Although an integration over time has been performed in the estimation of dose, it is important to understand that dose rate estimates may also be made using the time-derivative of eq. (1). In that case, the left hand side of eq. (1) will be a set of organ dose rates given as a function of time post-injection of the radiolabeled agent. Such exposure rates, if referring to a organ at or very near the body surface such as the liver, could be roughly measured using external probes.

We should point out that the traditional calculation using eq. (1) generates the mean dose to the target organ. The left-hand side may be shown to be the ratio of total energy absorbed divided by the mass of the target. This need not be the case in general. Statistical distributions of dose, in the form of dose-volume histograms, have been produced for internal beta emitters (Liu et al. 1998). Such results are analogous to histograms found in external beam therapy. Although not yet used extensively in treatment planning, such distributions may eventually prove to be important in both normal organs and tumors.

C. Properties of the S Matrix

1. Non-Penetrating (Charged Particle) Radiation

One may logically separate S values into S_{np} and S_p parts; these refer to so-called non-penetrating (np) and penetrating (p) radiation given off by the radionuclide of interest. Typically, the user assigns charged particle radiation to the former category and gamma and *x*-rays to the latter. Some emitters, such as ^{90}Y, are purely of the charged-particle type; these are of considerable interest in RIT due to the reduction in ambient radiation levels during therapy procedures.

If we assume that np radiation cannot escape from the source (and therefore target) volume, individual terms of S_{np} can be computed using the relationship:

$$S_{np} = (1/m) * 2.13 * \sum_{i=0,n} f_i E_i \tag{2}$$

where f_i refers to the probability of emission of *np* radiation of energy E_i . A factor of 2.13 is used when energy is in MeV and the organ mass term (m) in eq. (2) is in grams (g). In this overview, we have also explicitly neglected Bremsstrahlung radiation. Thus, S_{np} will only contain diagonal terms. The investigator can calculate this S_{np} matrix directly using eq. (2) given emission information and organ or lesion mass. We will describe below how to augment the computation if edge effects and/or Bremsstrahlung are to be considered. If these two corrections are included, the situation, by definition, becomes one in which the radiation is penetrating. Thus, use of the term non-penetrating is only an approximation.

2. Penetrating (Photon) Radiation

For photons, the value of S_p includes an additional term for the absorbed fraction (φ) of the ionizing radiation in the target organ of mass *m*:

$$S_p = (1/m) * 2.13 * \sum_{i=0,n} f_i E_i \varphi_i \tag{3}$$

Computations of S_p can be simplified if we consider an infinite homogeneous medium (Loevinger et al. 1991). In this case, the reciprocity theorem may be invoked to prove that S_p is a symmetric matrix (Loevinger et al. 1991). For anthropomorphic phantoms actually used in computing the penetrating part of *S*, this simplification can be shown to be only approximately true. The reader may test this assertion by inspecting off-diagonal elements of *S* for a photon-emitting radionuclide of interest (Snyder et al. 1975).

Tumor dose estimates for penetrating radiation represent a challenge since these tissues are not included in the standard set of source and target organs available to

the user. Macey has indicated a graphical method for estimating such *S* values if one knows the tumor mass and radionuclide (Meredith et al. 1993). A computer program for gamma dose estimates to spherical lesions has been developed by Johnson (1988). While such contributions to tumor dose may be small compared to the particulate component, it is important to find their magnitude in a given patient case. This topic is discussed in section VI.C.6.

D. Historical Background

Perhaps because radionuclide therapy with ^{131}I for thyroid cancer has been so successful and safe, there has been little historical incentive to provide a rigorous treatment planning approach for clinical radionuclide therapy practice (Hurley and Becker 1983). In addition, methods and technology, particularly computers, required to provide more accurate estimates were not available in Nuclear Medicine until the mid-1970s. The thyroid cancer patient has usually been treated on the basis of an empirical approach. As is the case for many RIT protocols, the treatment plan relies on an initial imaging study with a tracer amount of ^{131}I administered to search for remnant thyroid tissue and metastatic sites in the whole body. A more complete discussion of radioiodine therapy of the malignant thyroid is presented in section VII.

Over the past two decades, significant progress in medical technology has been made and the use of Computed Tomography (CT), Magnetic Resonance Imaging (MRI), and Single Photon Emission Computed Tomography (SPECT) imaging can yield most of the data required to provide more accurate patient-specific radiation absorbed dose estimates. Anatomic size, location, and volumes of organs and tumors can be provided non-invasively from CT, MRI, ultrasound, Positron Emission Tomography (PET), and SPECT images (Leichner et al. 1981). This should allow every patient to receive a customized therapy plan involving the administration of a specified amount of activity (Macey et al. 1991).

E. The Tracer Principle

In the present context, the tracer principle states that a relatively small (tracer) amount of a radiopharmaceutical can be used to predict the spatial and temporal distribution of a subsequent larger amount of the same radiopharmaceutical in the same patient. This principle has been used successfully in radionuclide therapy for thyroid cancer, although the uptake and distribution of ^{131}I in the thyroid patient has not been rigorously followed. The concept relies on the assumption that the response of the biological system is not perturbed by the diagnostic study.

$$\left[\frac{rad}{mCi}\right]_{therapy}^{tumor/organ} = \left[\frac{rad}{mCi}\right]_{diagnostic}^{tumor/organ} \tag{4}$$

Based on the tracer principle, the radiation absorbed dose/administered radioactivity to tumors/organs from a therapy procedure should be equivalent to the values calculated from a prior diagnostic procedure as given by eq. (4). Information from the tracer study is used to calculate the amount of activity required for a therapy procedure. A prescribed radiation absorbed dose to a tumor or dose-limiting organ usually dictates the amount of activity that can be administered by:

$$A_0[therapy\ mCi] = \left[\frac{D_{prescribed\ therapy\ dose}}{\left[\frac{rad}{mCi}\right]_{diagnostic}} \right]_{tumor} \tag{5}$$

A different definition of tracer is often used in Nuclear Medicine. In that context, the user assumes that a radiolabeled form of a molecule has the same biodistribution as the native or unlabeled molecule. This may or may not be true in the case of labeled antibodies due to changes in molecular weight and loss of label (particularly iodine) *in vivo*. Thus, our tracer concept is a more restricted one.

F. Treatment Planning for Radioimmunotherapy

Unlike ^{131}I therapy for the thyroid cancer patient, RIT is more toxic because a large fraction of the administered activity remains in various organs and spaces in the body. Although the fraction of the administered activity that localizes in tumor may be comparable to the concentrations of ^{131}I in many thyroid cancer patients after thyroidectomy, the remainder of the activity administered is not rapidly eliminated like ^{131}I. The design of a specific treatment plan for every RIT patient is important both for the safety of the patient as well as the protection of the staff and visitors. Radiation absorbed doses could in principle be measured with miniature dosimeters implanted in selected organ and tumor sites. However in practice this is impossible and therefore most dosimetry methods depend on acquiring *in vivo* pharmacokinetic data and deriving radiation absorbed dose estimates numerically.

Dose estimation plays the most important role in treatment planning. Using the tracer principle described above, the physicist will estimate absorbed doses to the important normal organs and to tumor site(s). In the latter case, the site must usually be visualized in the nuclear image in order that the dose be estimated. If this is not the case, only normal organ dose limitations will normally enter into the planning phase.

G. Toxicity and Efficacy

Today most clinical research protocols are designed to test and validate a hypothesis. The practical steps in a clinical trial of a new drug or procedure involve Phase I, II, and III trials. The Phase I trial is designed to establish the toxicity limit

defined as the maximum tolerated dose (MTD) in a small group of patients. Phase II trials are designed to test the efficacy of the same procedure in a small group of patients at a dose level somewhat lower than the MTD. Phase III trials usually involve multi-center studies with patients enrolled at various institutions and different investigators.

Although these steps are required for clinical trials with chemotherapy agents, radionuclide therapy trials can in principle be designed to combine the Phase I and Phase II steps. The radionuclide approach is especially valuable since it allows the investigator to predict to some degree the toxicity and efficacy of a radionuclide therapy procedure. For example, the biodistribution of the radiopharmaceutical in organs/tumors in the body can be obtained from serial radionuclide images obtained at various times after administration. Localization of the radiopharmaceuticals in specific organ or tumor sites can be used to determine whether the patient should proceed to the therapy step. If there is no tumor localization of the radiopharmaceuticals detected in the diagnostic images, the patient is less likely to benefit from the subsequent therapy and consequently should not have to be subjected to the unnecessary risk. All of these data are unique to nuclear techniques and are not found in the classical chemotherapy trial.

II. PROTOCOL DESIGN FOR RADIONUCLIDE THERAPY

A. What Biological Data are Required

Availability of good biodistribution data for a specific radionuclide therapy procedure allows the researcher to establish fundamental dose-response relationships. Simple questions such as what data are required to provide dose estimates can usually be answered from prior biokinetic information derived from animal—usually mouse—studies. Frequency of sampling blood, whole body, and normal organs can be estimated from the animal data. However, judicious design and collection of data are fundamental to providing reliable absorbed dose estimates in man. From the patient's standpoint, one should take into account that all data acquisition involves inconveniencing the patient and so a compromise must be made between limiting the amount of biological data collected and reliability of estimates that are calculated from that data.

B. Design of Dose Estimation Protocol for Radioimmunotherapy

Dose estimation protocols involve serial collection of whole body, blood, normal organ, and tumor data. The radiopharmaceutical is constantly moving from blood to various organs and compartments in the body. Schemes to track the

Table 2. Typical Data Acquisition Protocol Designed to Acquire Biokinetic Data Required to Provide Absorbed Dose Estimates for RIT Patients Receiving I-131 CC49

Biokinetic Data Acquired	Day 0, (End of injection is t = 0)	Day 1	Day 2	Day 3	Day 4
5 ml Whole Blood	15', 30', 1 h, 6 h	24 h	48 h	72 h	96 h
Cumulated Urine	0–6 h, 6–24 h	24–48 h	48–72 h	72–96 h	96–120 h
Tumor/Organ Imaging	1 h	24 h	48 h	72 h	96 h
Whole Body Probe	1h, 6 h	24 h	48 h	72 h	96 h
Biopsy of Tumor		24 h	48 h		

changing pattern of uptake and clearance in sufficient detail must be devised to provide good dose estimates. Table 2 illustrates a typical design of a dose estimation protocol for collection of biokinetic data from breast cancer patients enrolled in a RIT study with ^{131}I CC49. Some of these data can only be acquired via an *in vivo* imaging study; for example, by using a gamma-emitting radionuclide labeled to the CC49 antibody, such as ^{99m}Tc or ^{111}In or, alternatively, a low dose of ^{131}I CC49 prior to therapy. We will describe below a method of using the diagnostic study with one radionuclide to predict the therapy outcome with a second radionuclide attached to the same pharmaceutical.

C. Dose Estimation in Humans from Murine Biodistribution Data

We first consider a sample computation of human dose estimates based on murine (obtained from laboratory mice or rats) data. Most of these analyses involve immune-deficient (nude) mice in the case of RIT. This type of analysis is often used in the Investigational New Drug Application (IND) application to the Food and Drug Administration (FDA). Unless such estimates can be supplied, approval for human use of the radiopharmaceuticals will, in general, not be given.

The murine model used in such biodistribution analyses should be of normal, tumor-free animals. Normalized counts are obtained from NaI(Tl) counter measurements using an energy window appropriate for the gamma energy of the radionuclide. Data taken would include percent injected dose (PID) as well as

corrected uptake in percent injected dose per gram of the tissue (PID/g). These measurements are tabulated as decay-corrected biodistributions in various organs and at a number of time points after injection of the radiolabeled material. Whole body accumulation may additionally be measured using a single or paired probe system set at a fixed distance from a constrained animal. As described below, a mathematical picture of the biodistributions is helpful in determining the total area under the curve of each source organ. In this example, we will consider using a single exponential model to represent organ data. The resultant **biological** half time ($T_{1/2b}$) is combined with the physical half life ($T_{1/2p}$) to obtain the effective half time T_{eff}:

$$T_{eff} = \frac{T_{1/2p} * T_{1/2b}}{T_{1/2p} + T_{1/2b}} \tag{6}$$

The residence time τ for a tumor/organ in the mouse that clears with an effective half time T_{eff} is given by:

$$\tau_{tumor/organ} = 1.44 * T_{eff} * PID_{t=0} / 100 \tag{7}$$

where the indicated PID is the percent injected dose at end of injection for a mono-exponential compartment and T_{eff} is the effective half time in hours. This area under the curve has the injected activity divided out so as to be in pure time units; the resultant value is the residence time (τ) of the source organ. A set of such times is the residence time vector for murine estimates. In the case of animal biodistribution data, there may be 10 or more individual organs or tissue compartments to consider for this vector.

To estimate the residence time in a human from the biokinetic results in the mouse, we use a mass correction factor to account for the different ratios of organ to total body weights in the mouse and in man. To first order, we assume that the uptake in a given organ, in PID, depends only on the ratio of organ mass divided by the total body mass. To correct for differences in this apportionment ratio between murine and human species, we can use the following:

$$CR = \frac{\tau_{man}}{\tau_{mouse}} = \frac{\left[\dfrac{organ\ mass}{total\ body\ mass}\right]_{man}}{\left[\dfrac{organ\ mass}{total\ body\ mass}\right]_{mouse}} \tag{8}$$

This process is essentially an organ correction factor (CR) for differences in relative perfusion between the mouse (or other animal) model and the human subject. Usually the biokinetic data from the mouse are provided as PID/g, which simplifies this conversion for dose estimation since the murine organ mass is included in the data set. An example of this type of calculation is given in Appendix A. These

correction factors are often sizeable and should be applied when using animal data to predict human results.

III. CLINICAL ASPECTS OF RADIOIMMUNOTHERAPY TRIALS

A. Patient Eligibility

Radioimmunotherapy trials are usually fairly demanding for the patient. A number of additional constraints are placed on the individual and his/her tumor type beyond those found in radionuclide therapy. In general, RIT patients must have a good performance status, defined as a Karnofsky scale above 60% and no other severe systemic disease (Press et al. 1989, Breitz et al. 1992). Only patients with tumor types known to be reactive with the antibody are to be considered. This may be done with peroxidase staining of tumor tissue samples obtained from the patient. Alternatively, an *in vivo* imaging study may be performed with a gamma-emitting radionuclide label to demonstrate uptake in one or more known lesion sites (Breitz et al. 1993, Eary et al. 1990). Additionally, if the antigen is secreted into the blood, such as carcinoembryonic antigen (CEA), a blood assay may provide the needed tumor specificity. In the latter case, the test is done with less cost than that requiring tumor samples. In the event that the patient's tumor is antigen-positive, a life expectancy of at least 2 months is necessary so that adequate monitoring of normal organ function and tumor response can be assessed during the radiotherapy protocol.

On entry into the study, good performance status is important because the monitoring of the patient for the dose estimation data is demanding. Generally the protocol will require several sessions of nuclear imaging, of one to two hours each, depending on the gamma camera system. SPECT studies require that the patient be able to lie flat with arms raised for a sufficient length of time (perhaps 20 minutes) for an adequate study to be acquired. This may be at one time point only for a qualitative assessment of tumor uptake. Some investigators will use SPECT for quantitative estimation of activity in tumor masses and/or normal organs at one or more times. For older patients or patients with pulmonary complications, this may be an unrealistic expectation.

Good performance status may also be essential because of the high levels of internally administered activity. Slow excretion of the radiolabeled antibody metabolites pose radiation hazards similar to those from patients receiving high dose ^{131}I for treatment of thyroid disease. Exposure to medical personnel will depend on the radionuclide administered. To reduce such exposure hospitalized patients should be able to care for themselves with minimal nursing care required. Patients with lymphoma receiving high dose ^{131}I radiolabeled antibodies have even been trained to collect their own blood samples (Press et al. 1989). Patients should

be capable of collecting their urine and measuring the volume themselves if this is required in the protocol. Because of radiation hazards, incontinent patients should not be studied under these conditions.

Baseline blood tests confirming adequacy of bone marrow, renal, and hepatic function must be obtained. The patient must not have received chemotherapy or radiation therapy for at least 4 weeks prior to radiolabeled antibody treatment to allow full recovery from side effects of those treatment modalities. Tumor size must be documented by conventional diagnostic techniques (physical examination, planar film, CT image, MRI scan or ultrasound) so that response can be monitored. At present, trials in patients with unmeasurable disease to detect the value of RIT as adjunctive therapy are infrequent, although at least one colorectal cancer adjuvant trial has reported beneficial results using unlabeled antibody (Riethmuller et al. 1994).

If patients have had prior exposure to a murine or other antibody, circulating titer against that antibody must be measured. Presence of such a human antibody to the clinical agent may exclude the patient from participating in the study. Inclusion of such patients often results in the resultant radioactive antibody-antigen complexes going directly from the blood to the liver with little activity seen at the tumor sites.

When the patient has met all the eligibility requirements and signed informed consent, additional preparation may be necessary before receiving the labeled antibody. For example, patients receiving ^{131}I-labeled antibodies must, in addition, have their thyroid gland appropriately blocked using Lugol's Solution. Patients also should be hydrated to reduce kidney and bladder effects due to radiation. If gastrointestinal excretion is significant, cathartics should be administered to reduce gastrointestinal mucosa exposure during fecal excretion of the iodine label. A summary of the required pre-study clinical evaluation is shown in Table 3.

Radiolabeled antibody must not be administered until the quality assurance studies have been reported. These tests must show adequate assessment of purity, potency, and safety. These could include an endotoxin assay, Instant Thin Layer Chromatography, and High Performance Liquid Chromatography (HPLC).

Emergency supplies must be readily available in case of an allergic reaction. These would include diphenhydramine, epinephrine, and steroids. Patients have vital signs monitored immediately prior to injection and regularly thereafter.

B. Administration of Radiolabeled Antibody

Radiation precautions must be observed for the infusion of the radiolabeled antibody. Gloves and protective glasses must be worn while handling the radiolabeled antibody. When the radioactivity is to be infused slowly, the syringe is placed in a Lucite™ and lead-covered infusion pump (Williams et al. 1995a). When a bolus injection is required, a shielded syringe is used. All couplings and connections in the

Table 3. Pre-Study Patient Evaluation for Radioimmunotherapy

- History and physical exam
- Histologically confirmed diagnosis of antigen presence on tumor by histology or imaging study. Blood assay may be used if antigen is shed.
- Chest X-Ray, Ultrasound, CT scan or MRI scan for lesion size
- Biochemical Profiles;
  - Complete blood count (CBC)
  - Chemistry Screen
  - Urine Analysis
  - Prothrombin Time (PT)
- Pregnancy test if applicable
- Signed informed consent
- Baseline Human Anti-Mouse Antibody (HAMA) or other appropriate human antibody

line between the source and the patient must be tested prior to beginning the injection procedure. Medical personnel must take appropriate precautions in case of contamination or spills. Absorbent pads are placed under the lines and on the floor below the bed in case of spills. A more complete discussion of radiation safety aspects of RIT is included in section IX. Many of the above restrictions apply to the general case of radionuclide therapy.

Success of this treatment modality depends upon sufficient radioactivity being carried by the antibody to the tumor site(s). Several routes of administration have been used. Figure 1 contains a summary of these methods.

1. Intravenous Injections

This is the most commonly used procedure for administration of radionuclide therapy to patients. Two intravenous lines are established, one for administration of the radiolabel and one for post-injection blood sampling. The latter may be retained during the course of the therapy to provide the required samples as described below in paragraph 4. Duration of injection will vary from several minutes to several hours depending upon adverse reactions and the amount of protein used in the therapy.

2. Intraperitoneal Injections

Additional factors for intraperitoneal RIT studies must be considered (Jacobs et al. 1993). Radiological examination is not sensitive enough to define the extent of the disease. An open laparoscopy or a laparotomy performed within one month of the study will give the most reliable data, although even this may not provide

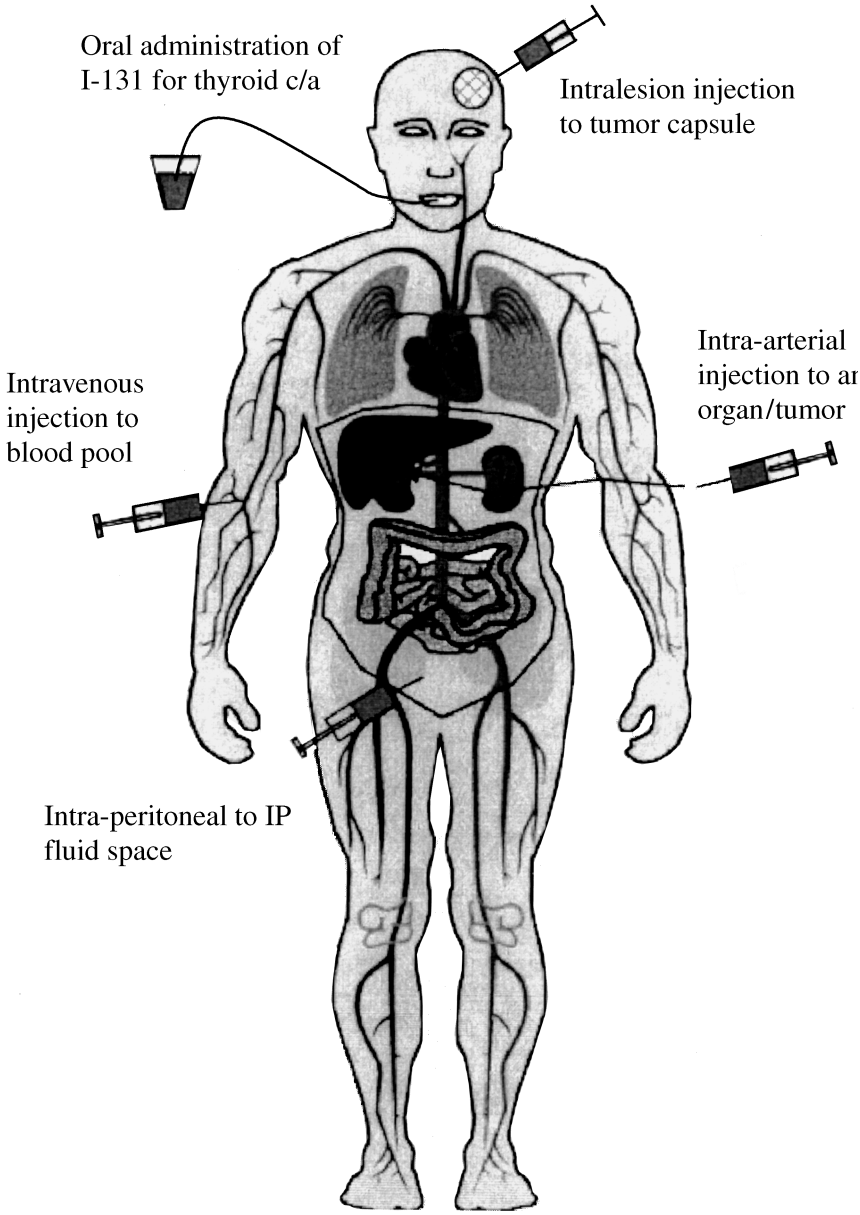

Figure 1. Routes for administration of radiopharmaceuticals to a therapy patient.

complete information. Serum markers may also be used as a guide as to the extent of disease and response.

Prior to administration of a large dose of radioactivity, the peritoneal cavity access must be evaluated to be sure that the radiolabel will distribute throughout the volume. A ^{99m}Tc-sulfur colloid study may be performed to assess this; activity must be seen in the pelvis and paracolic gutters. When severe ascites is present, as much ascites fluid as possible must be drained prior to the infusion. The radiolabeled antibody may be administered through a porta-cath or Tenckhoff catheter. The volume of fluid administered with the antibody should be sufficient to allow distribution throughout the peritoneal cavity. This volume can range from 300 ml to 1000 ml of normal saline or Ringer's lactate. The patient is instructed to roll 360 degrees three times prior to the gamma camera imaging. Later, they are encouraged to move about freely to promote uniform distribution. To estimate clearance of radioactivity from the peritoneal cavity, and to estimate absorbed dose to the peritoneal surface, aspiration of peritoneal fluid samples is desirable.

3. Intra-Arterial Injections

Known metastases must be confined to one region that can be perfused by intra-arterial injection. On the day of the radiolabeled antibody injection, a catheter must be placed under fluoroscopy into the artery perfusing the area of interest. The catheter is removed following the injection. Additional monitoring is required for adverse events resulting from catheter placement.

4. Intralesional Injections

This is a more invasive and time-consuming technique and can require hospitalization for several weeks. For example, in the treatment of gliomas, a catheter is placed in the lesion at craniotomy, or by stereotaxy some days later. This catheter is placed in the residual cavity after as much tumor as possible has been resected. Removable or indwelling catheters may be used. A reservoir may be connected to the catheter and placed under the skin for repeated injections (Riva et al. 1994).

We should point out that this approach has been followed in the case of radionuclide therapy of pancreatic carcinomas. Here, a local anesthetic is used and a 22-gauge needle inserted into the lesion under CT guidance. Aggregated albumin (MAA) is given initially with a follow-on dose of ^{32}P to yield the desired absorbed radiation dose estimates (Order et al. 1994). Imaging of the lesion may be performed using the Bremsstrahlung radiation from the single concentrated source of radiophosphorous.

C. Patient Monitoring After Radiolabeled Antibody Administration

Patient monitoring must be done under the supervision of a physician. Patients are observed for acute allergic reactions such as flushing and hives. Adverse reactions must be treated and reported as required in the protocol. An assessment for allergy may be done using a small test dose of the protein to be injected. A 5 microgram amount can be injected subdermally and the site observed for 25 minutes to determine any sensitivity. If swelling and other reactions are seen, injection of the larger imaging or therapy dose (typically 5 milligrams of protein) can then be prevented. Vital signs must be monitored for at least one hour post antibody administration.

To obtain data for dosimetry estimation, imaging should begin immediately following injection and prior to voiding to assess the baseline activity. When high dose ^{131}I is administered, imaging may begin only after the activity level has decreased to values on the order of 30 mCi or less. This restriction is based on current state and federal regulations that are designed to reduce radiation exposure to hospital personnel and also because the Anger camera is only designed to detect relatively low amounts of radioactivity in patients. High count rates may lead to dead-time effects including spatial location errors and count losses so as to make quantitative imaging difficult.

Biochemical and hematological parameters are monitored regularly for 3 months or longer following the study. Typically, biochemical changes are not significant. With increased levels of radioactivity administered, bone marrow suppression is observed as a reduction in the number of white blood cell and/or platelet counts from baseline values. With increased radioactivity, these counts will drop earlier and to a lower level. The platelet count decreases approximately a week earlier than the white cell count—usually at week four.

Levels of patient antibody to the injected protein are assessed for up to 6 months. In the case of a murine antibody, the human response is termed a Human Anti-Mouse Antibody or HAMA. Similar acronyms such as HACA and HAHA refer to human anti-chimeric and human anti-human antibodies respectively. It should be noted that the patient may also develop antibodies against the chelator used to attach radiometal to an injected protein. In any event, these titers should be determined weekly for 6 weeks and then monthly. Presence of elevated levels of human antibody may preclude repeat treatments.

At a specified time, usually 6 to 8 weeks, a follow-up radiological exam is performed to assess tumor response. Generally, this would be a CT or MRI image so that the tumor volume(s) post-therapy may be compared directly with the baseline study. Nuclear bone scan images may be used to evaluate the progress of therapy on bone metastatic sites. Such evaluations would also be appropriate for general radionuclide therapy treatments.

D. Repeat Injections of the Same Antibody

Prior to repeat administration of antibody, serum human antibody levels must be measured. In patients with lymphoma, cycles of radioimmunotherapy can often be administered. In patients with other tumors who have received murine monoclonal antibodies, elevated HAMA levels generally preclude a subsequent administration. In Phase I studies, human anti-antibody levels must be monitored until the characteristics of the patient response are known.

E. Protein Preloading

Early studies with radiolabeled antibodies established that a minimum mass of a foreign protein was required for administration into the blood. This followed from the fact that various receptor sites in the liver, lung, and other normal tissues must be saturated before the concentration of the radiopharmaceutical in the blood was high enough so that antibody would localize in the tumor. For lymphoma, a few mg of protein were found to be adequate. Literature studies have pointed out that there may (Patt et al. 1988) or may not be (Wong et al. 1998) an advantage in increasing the amount of injected protein above this minimal level. Some protocols, because of significant levels of circulating antigen, require relatively large amounts of unlabeled protein prior to the injection of the labeled antibody (Breitz et al. 1992, DeNardo et al. 1990).

It should be mentioned that increasing the injected amount of protein has two possible negative results. First, the likelihood of patient antibody response will increase with the amount of injected foreign antibody. In addition, the cost of large amounts of engineered protein may preclude such procedures. For example, in mice, about 700 μg of antibody were required to significantly reduce an anti-CEA antibody's hepatic uptake (Beatty et al. 1989). Scaling these results to man implies clinical injected protein doses approaching one gram. No one has yet attempted such injections in solid tumor therapy although values on the order of several hundred milligrams have been required in treating hematological malignancies due to circulating antigen in the blood or high levels of B-cell antigens on lymphoid tissue (DeNardo et al. 1990).

Most RIT patients receive their radiopharmaceutical as an intravenous injection that is either infused over a planned time or injected as a bolus. Localization of the radiolabeled antibody in the target tumor tissue and normal organs is a continuous process of uptake and clearance and the pattern observed is the net result of inflow and outflow from sites that are visualized on a radionuclide image. Intravenous and intra-arterial routes depend on the assumption that the radiopharmaceutical can leave the blood pool and enter the various volumes or partitions in a tumor. In the case of intraperitoneal injection, radioactivity enters the lesion sites directly from the peritoneal fluid as well as from circulation. In the latter case, there is a significant time delay before the material enters into the blood circulation.

IV. ACQUISITION OF PHARMACOKINETIC PATIENT DATA

A. Biological Data of Interest

The activity and concentration of the radiopharmaceutical in all major source organs and spaces in the body must be determined for the dose calculation step. Usually the activities in whole blood and whole body are simple to acquire while tumor and organ uptake measurements require quantitative organ imaging procedures.

1. Blood Activity

Changing activities in whole blood and plasma are determined from serial blood samples acquired at various times after administration of the radiopharmaceutical. Usually 3 to 5 ml of blood are collected at 1, 4, 24, 48, and 72 hours from a vein in the limb opposite to that in which the radiopharmaceutical was administered. Other schedules may be used with animal data providing some predictions as to human blood kinetics. In addition, the pharmacokinetic modeling program (see below) can be used to predict optimal times for blood sampling. These times, however, may not be convenient for patient or clinical logistics.

2. Whole Body Retention

This information can be measured most conveniently with a probe placed at 2 to 6 meters from the surface of the patient as shown in Figure 2. Here, one obtains a reading for the count rate from the patient about 10 to 20 minutes after the activity is administered and prior to any excretion via urine or feces. This initial value is used to normalize all subsequent measurements made in the same geometry. The assumption of this approach is that the sensitivity of the probe or dosimeter used to measure the various readings is reasonably independent of where the activity is located within the patient.

Because of the redistribution of the activity over time, it is best that a pulse height analyzer be used in conjunction with the probe system. Exclusion of scattered radiation from the patient is the primary motivation for this strategy. Thus, as we describe below for gamma cameras, an energy window should be set up over the photoelectric peak of the detected gamma radiation.

A second method for monitoring whole body retention is a sequence of whole body images taken with a gamma camera in scanning mode. Generally, these images will include regions from the top of the head to the knees with the arms being visible at the sides of smaller patients. As in the probe case, positioning of the patient for repeat scans will require a localization method. One technique is the use of wall-mounted lasers to reposition the patient serially. This method has

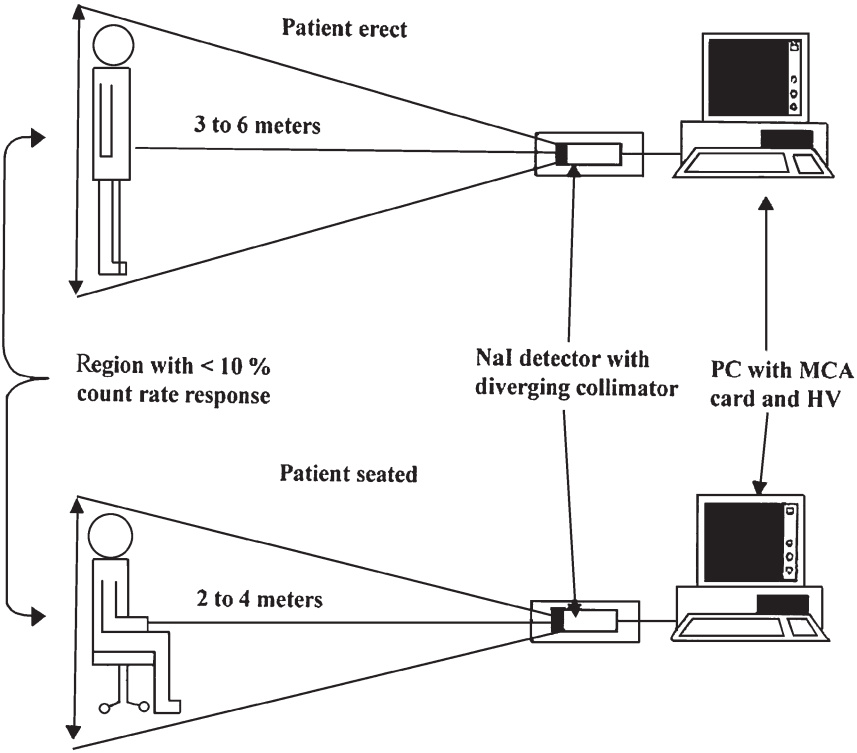

Figure 2. Measurement of whole body retention of activity with probe detector.

the advantage that distributions within patient organs can be acquired at the same time as the whole body image(s).

3. Other Normal Organ and Tumor Activity

Activity in normal organs and tumor is most conveniently determined from a quantitative Anger camera image. Special acquisition protocols must be used to calculate activity from the number of counts detected in a specified organ or tumor site that is visualized in the radionuclide image. Magnitude of activity in a given organ is often referred to as uptake and is usually measured in percent injected activity (PIA).

Uptake in a tumor or organ is most readily estimated if the number of counts/pixel (count density) detected from that region in the Anger camera image exceeds the count density in the immediate vicinity. A tumor near high count density regions such as the liver and cardiac volumes requires a much larger ratio of uptake

compared with tumors in the limbs and skull. Most region of interest (ROI) methods used for scoring uptake from these images rely on drawing a background region in the immediate vicinity of an uptake site or a contralateral region of the body if the background surrounding the uptake region is not uniform. These background subtraction techniques are designed to remove the contribution of counts to a tumor/organ site from radioactivity in overlying and underlying tissue.

4. Minimal Levels of Uptake for Visualization

Simple statistical analysis methods can be used to determine the minimum number of counts that are required to visualize the typical level of uptake of radiolabeled antibodies in tumors. Usually the concentration in a tumor must be several times greater than the concentration in the immediate vicinity to make the tumor visible in a planar Anger camera image. Biokinetic data indicate the typical range for human tumors is about 0.001 to 0.02 PID/g (20% ID/kg). For a 20 g tumor in a patient, these levels of uptake would be translated to 0.020 to 0.40 PID. If the patient receives 10 mCi ^{131}I labeled antibody for the diagnostic study, the 20 g tumor would be expected to have an uptake of 2 to 40 μCi (1.5 MBq). Whether this range of uptake is visualized in a whole body scan or a planar image depends upon multiple factors such as the background count density, physical decay, sensitivity of the camera-collimator system, and observer training.

Planar image acquisition times of 10 to 20 minutes are required to visualize tumor sites in RIT patients. These long times and the requirement for repeated images make it important to have a dual-head Anger camera with a large field of view. Generally, a whole body scan image is acquired to characterize the distribution in the whole body followed by a series of conjugate image sets that include expanded views of chest, abdomen, and pelvis. If available, laser methods should be used to register the patient for a set of serial images.

B. Uptake Measurements *in Vivo*

1. Attenuation Corrections

All uptake measurements depend upon correction of recorded data for background and attenuation in the patient. Several strategies exist for these corrections. In the single projection image method, which can be used for superficial uptake sites, the attenuation correction factor can be set to unity. Here the uptake is given simply by:

$$A_{tumor/organ}[Ci] = \frac{N_t[counts]}{\varepsilon[counts / Ci\ s] * \Delta t[s]} \tag{9}$$

where ε is the efficiency of the camera and collimator system and N_t is the number of counts recorded in time Δt.

For the conjugate view approach, the user must obtain, essentially simultaneously, two diametrically opposed views of the same object (Thomas et al. 1976, Sorenson 1974). Figure 3 contains a geometric description of the process. The number of counts detected from the anterior (N_{ap}) and posterior (N_{pa}) projection images of an organ of thickness ℓ cm in the body, with overlying and underlying tissue thicknesses a and b cm is:

$$\frac{N_{ap}}{\Delta t} = \varepsilon * \frac{Ae^{-\mu a}}{\mu \ell}\left[1 - e^{-\mu \ell}\right]; \quad \frac{N_{pa}}{\Delta t} = \varepsilon * \frac{Ae^{-\mu b}}{\mu \ell}\left[1 - e^{-\mu \ell}\right] \tag{10}$$

The geometric mean of these values becomes:

$$GM = \sqrt{N_{ap}N_{pa}} = \varepsilon * \Delta t * Ae^{-\mu(a+b+\ell)/2}\,\frac{\sinh(\mu\ell/2)}{(\mu\ell/2)} \tag{11}$$

For organ thicknesses that are sufficiently small, the source thickness factor $(\mu\ell/2)/\sinh(\mu\ell/2)$ can be set to one. This simplification is often the basis for using the geometric mean of counts to estimate organ and tumor uptake from conjugate view Anger camera images. The geometric mean of anterior and posterior image counts can provide an estimate for tumor/organ uptake very simply from a measurement of the total thickness ($a + b + \ell$) of the body region in which the organ is imaged. We refer to this as the total thickness T. The linear attenuation coefficient is defined as μ in the above equalities.

The attenuation factor in the above equation for the GM can also be determined from a transmission source imaging technique. If the transmission and emission sources have similar μ values, the activity in an organ can be calculated using:

$$A_{tumor/organ}[\mu Ci] = \frac{\sqrt{N_{ap}N_{pa}}}{\varepsilon * \Delta t}e^{+\mu(a+b+\ell)/2} = \frac{\sqrt{N_{ap}N_{pa}}}{\varepsilon * \Delta t}\sqrt{\frac{N(0)}{N(T)}} \tag{12}$$

where $N(T)$ is the number of counts with the patient between source and gamma camera and $N(0)$ is the number of counts without the patient in place. Source thickness factor has been set to unity in eq. (12). The transmission emission approach can be invoked to estimate uptake of most gamma-emitting radionuclides currently used in nuclear medicine to an accuracy of about 10% to 20% (Macey and Marshall 1982). If the radionuclide used to determine the attenuation correction factor emits a different energy than the therapy radionuclide (e.g., if ^{57}Co is used for the transmission measurement in a patient who received ^{131}I for RIT), special correction factors are required to account for the differences in tissue linear attenuation coefficient values.

Transmission scan set-up for static or whole body image acquisition

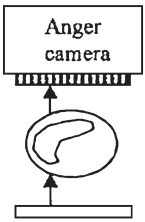

Cross-section through organ in body of uniform or non-uniform tissue

10 - 20 mCi Co-57 flood source at 40 cm

Procedure:

1. Acquire N(0) image
2. Acquire N(T) image
3. Find ACF for each organ/tumor site

$$ACF_{ROI} = SQRT[N(0)/N(T)]$$

Set-up for acquisition of geometric mean images and procedure

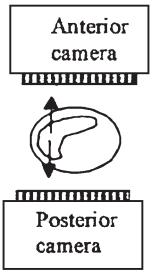

Cross section of organ in body with radioactivity

Procedure:

1. Acquire GM images
2. ROI counts after background subtraction
3. Multiply GM counts by ACF from Transmission study

$$GM_{ROI} = SQRT[(N_{AP} - bgd)*(N_{PA} - bgd)]$$

$$Activity_{ROI} = GM * ACF/sensitivity$$

Figure 3. Acquisition of transmission and emission images. ACF is the attenuation correction factor.

2. *Scatter Correction Techniques*

In the above analyses, the photons were assumed to travel in such a manner that scattered radiation did not enter the camera or other detector system. Scatter correction is usually necessary because the recorded counts in a given camera pixel will include primary as well as scattered photons.

Typical scatter corrections have included using adjacent areas on the planar image to subtract such counts or the use of variable windowing on the gamma camera photon spectra to exclude lower energy photons from the imaging. For a single photon emitter such as ^{99m}Tc, this would entail setting two energy windows: one over the direct photons at 140 keV and one over the scattered radiation at 100 to 120 keV. A subtraction of the latter from the former gives the net direct (unscattered) counts for that region of the patient. This is discussed in greater detail in the section on quantitative SPECT imaging. Use of a triple-energy window (TEW) with satellite windows set both above and below the photopeak has been described (Ichihara et al. 1993). A weighted average of the count rates in these two satellites is then subtracted from the count rate in the center of the spectrum to produce a primary count rate.

If the radionuclide used in the imaging procedure emits more than one photon, these strategies for spectroscopic scatter correction become more complicated. For example with ^{111}In, the dual-window program would require a total of four energy windows to be set. Yet the lowest of these, at 140 to 150 keV, would contain both scattered photons from the higher energy peak at 247 keV as well as scattered photons from the lower peak at 174 keV.

It is important to understand that because a pulse is recorded with a lower energy than the photoelectric peak in the detector does not necessarily indicate scattering. This ambiguity occurs due to the finite energy resolution of the NaI(Tl) crystal in the gamma camera. Direct photon energies appear to spread around a mean value with a full width at half maximum (FWHM) of approximately 10% or higher. Thus, correction using such secondary windows is uncertain and necessarily leads to loss of counts attributable to unscattered (direct) photons. Scattering within the crystal of the camera is also ignored in this analysis. A sample gamma camera photon spectrum for ^{111}In is shown in Figure 4.

Comparisons of the various types of spectroscopic scatter-correction techniques have shown (Ljungberg et al. 1994, Buvat et al. 1995) that no single method is best under all possible circumstances. One can conclude that some correction, however, must be applied to the acquired camera data.

Another method to include the effects of scattered radiation is to insert a buildup factor (B) into the counting equation. Thus, eq. (10) would have a revised anterior projection given by:

$$\frac{N_{ap}}{\Delta t} = \varepsilon \frac{A * B}{\mu \ell} e^{-\mu a}\left[1 - e^{-\mu \ell}\right] \tag{10a}$$

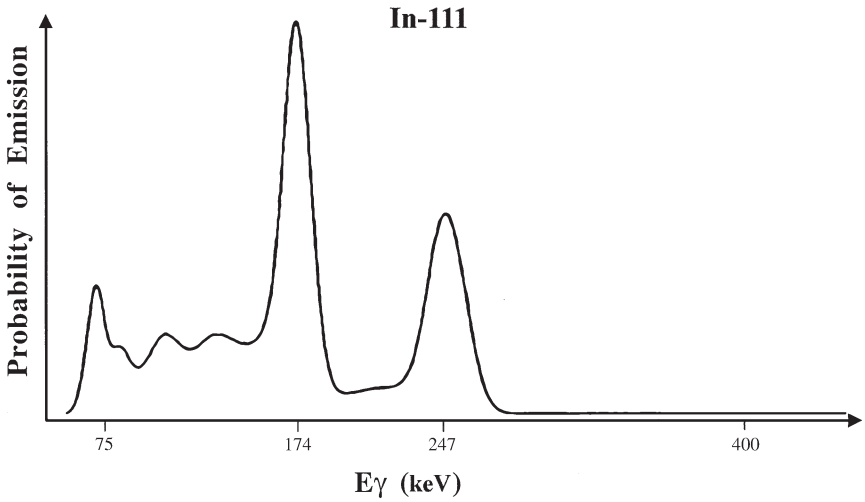

Figure 4. Photon spectrum from a gamma camera for ^{111}In.

An analogous change would occur for the posterior projection. In the original derivation by Thomas et al. (1976), the B factor was set equal to unity. Siegel and coworkers have determined such B functions for a variety of radionuclides by doing single source attenuation experiments with a set of tissue-equivalent phantoms (Wu and Siegel 1984). One may use either a depth-dependent or depth-independent value for B given the radionuclide (van Rensberg et al. 1988).

An artificial neural network to compensate for scatter and attenuation has been proposed as an additional method of correction (Maksud et al. 1998). The network learning time was found to be reduced if a geometric mean was used as the input data to the system.

3. *Use of Geometric Data from Anatomic Imaging*

As indicated, geometric thicknesses specified in the above equations may be determined using transmission nuclear imaging. There are at least two arguments, however, why a hybrid analysis, with both anatomic and physiological images, could be used instead. First, distances, organ sizes, and positions can now be rigorously established. Such data, typically obtained via CT scan, are required for the assessment of patient disease in the case of malignancy. Second, there is now no need of external transmission sources with their added patient exposure and cost (van Rensberg et al. 1988). In the case of anatomic information, the attenuation equation is expressed in the integral form:

$$\frac{N_i}{\Delta t} = \varepsilon \cdot \int a_i(x) B(x) e^{-\mu x} dx \tag{13}$$

where N_i are the counts recorded along the *i*th ray through the patient and $a_i(x)$ is the unknown linear activity density (μCi/cm or MBq/cm) at the depth x along that ray. Other factors in the equation have been defined previously. Liu et al. (1996) have solved the equation set (13) with a CT-assisted matrix inversion method (CAMI). By imaging a phantom with both CT and nuclear camera, these authors reported errors in three pseudo organ uptakes of between 5% and 15%. Using the geometric mean (GM) approach and the same phantom, comparable errors were on the order of 30%. Background activity was included in the phantom as a fourth radioactive source.

Other observers, using a humanoid phantom, have reported geometric mean activity estimates with errors on the order of 30% (van Rensberg et al. 1988). This uncertainty is one of the primary reasons why GM analyses must be carefully utilized. A second reason is the possible lack of a geometric mean value if the source can only be viewed from a single projection. It is important to recognize that the GM analysis also depends upon observing the organ clearly in both projections—without overlap of other tissues. For example, the right kidney and liver interfere with each other in almost any projection so as to make geometric mean activity measurements for these two organs difficult if both show accumulation of the radiopharmaceutical. Thomas and co-workers have indicated methods, involving hyperbolic functions, to account for other organs in the field of view (Thomas et al. 1988). These methods require use of lateral images to determine thicknesses of the tissues involved. A general review of uptake measurements, involving both non-scatter and scatter situations, is found in MIRD Pamphlet 16 (Siegel et al. 1999).

Finally, it should be emphasized that because a hot spot appears in a comparable location in two opposed projections there is no guarantee that it is the same source. For example, a tumor may appear in the lower left quadrant in the anterior view, but the spleen may be the strong uptake source seen in the corresponding position in the posterior projection. By using CT data and merging that image with nuclear camera information, this last kind of confusion may be reduced.

Table 4 contains a summary of the methods to evaluate organ uptake of radioactivity. Three logical cases are possible for the nuclear projections. The observer

Table 4. Non-SPECT Methods to Determine Organ Uptake in Nuclear Medicine

	Method		
Available Projection(s)	**GM**	**Single Image**	**CAMI**
Diametric Opposed	Yes	Yes	Yes
Single Projection	No	Yes	Yes
None	No	No	Yes

Note: CAMI means CT-assisted matrix inversion and requires the fusion of coronal CT (or MRI) projections and coronal nuclear images.

may have diametrically opposed projections, a single projection, or no nuclear image at all (!). This last case occurs when a CT or MRI image reveals a site that does not show enough contrast to be imaged by the nuclear camera. Those doing uptake measurements will have to deal with each of these three cases.

4. *Quantitative SPECT Imaging*

If a lesion or organ can be encompassed by a single set of SPECT images, these cross-sectional counts may be used to estimate uptake (Chang 1980). In this analysis, scatter corrections are applied to the reconstructed section or to each projection obtained over the angular interval (typically 360 degrees). As Ljungberg and Strand (1990) have indicated, the scatter corrections are generally done in one of two ways. Either the observer sets a secondary energy window over the Compton energy peak in the spectrum (as described above), or a convolution analysis is employed to determine the amount of scatter within the photoelectric energy window.

In the former case, two images are acquired at each angle over the range of detector rotation. Explicitly, we find a corrected projection count value via:

$$N_{pr} = N_{total} - kN_{sc} \tag{14}$$

where N_{pr} represents primary counts and N_{sc} are counts recorded in a scatter window. The constant k, called the scatter multiplier, is the ratio of scatter counts detected in the photopeak and scatter windows respectively.

This simple dual energy window scatter subtraction method was originally developed for SPECT images (Jaszczak et al. 1984). The method was found to be accurate to within 10% for ^{99m}Tc. With a photopeak window set at 127 to 153 keV (±10%) and scatter window at 92 to 125 keV, a k value of 0.5 was empirically determined. Both line sources and cold spheres were used in the measurements.

Koral and co-workers (1990) have extended the k-factor analysis to individual projection images. Here, somewhat different values of k were determined using only radioactive sources of ^{99m}Tc. In their study, k varied between 0.73 to 1.29 depending upon the geometry of the source and the size of the ROI selected by the investigator. Thus, it is clear that the user must determine a correction constant appropriate for the local camera and collimator system.

In the convolution technique, which requires only a single photopeak image set, a similar equation has been applied.

$$N_{pr} = N_{total} - Q \otimes N_{pr} \tag{15}$$

where Q is a scatter function and $\otimes$ the convolution symbol (Axelsson et al. 1984). Generally, Q is represented by a monoexponential function of counts versus distance off axis in a 22-cm diameter cylinder. Subsequently, Q has been found to be

non-stationary and, consequently, the method cannot provide the same accuracy as the dual energy window approach. A general review of quantitative SPECT imaging should be consulted for more details of the various scatter-correction methods (Rosenthal et al. 1995).

C. Organ and Tumor Volumes

The accuracy of determining tumor/organ volumes is important for dosimetry, since dose is a measure of energy density. One usually requires the anatomical volume of an organ or tumor site. Because this is a challenge for most nuclear medicine techniques, we must use volumes furnished by CT and MRI. Such volumes are also used clinically to determine the progress of the malignancy in the patient. While several imaging methods can be used, we should point out that palpation may be sufficient for external (skin) lesions.

1. Palpation

Palpation has been a classical approach to estimating volumes of surface lesions/organs in the clinic. The physician usually records the length (l), height (h), and width (w) of an abnormal lump (e.g., a lymph node), usually indicated by the patient, and the volume is calculated simply from the relationship:

$$V_{tumor} = \frac{4}{3}\pi\frac{(l * w * h)}{8} \tag{16}$$

This subjective approach is simple and easy to apply, and can be valuable for assessing the "hardness" and response of superficial nodes in various regions of the body. An example of this sort of volume estimation using CT data is given in Appendix B.

2. Imaging Methods to Determine Organ Mass

More objective volumetric methods rely on CT, MRI, and ultrasound to provide size estimates of organs and tumors in the body. These data can be used to provide organ/tumor-specific dose estimates (cf. section VI) and serve as a criteria for evaluating response based on serial imaging. Organs and tumors that have diseased/necrotic volumes may not localize a radiopharmaceutical equally in all regions. Sometimes this variation is due to poor perfusion. This can often be demonstrated in large tumor volumes where the necrotic segment can represent a significant fraction of the measured volume. Radiation dose estimation requires determining the functioning volumes inside these organs/tumors.

Radionuclide tomography can provide information for larger organs and tumors, and PET and SPECT can be used to measure the functioning volumes for organs and tumor sites larger than 10 ml. Biopsy with autoradiography can provide information on the microscopic distribution/fraction of a tumor/organ in which a radiopharmaceutical is distributed. This method is usually impractical for dose estimation because it is invasive and very localized. Biopsies in animal studies have demonstrated the distribution of protein agents to be heterogeneous. The longer range of energetic beta emitters tends to compensate for the heterogeneity and can be used to justify their use in clinical therapy.

V. DATA ANALYSIS METHODS

A. Activity and Percent Injected Activity (PIA)

Methods used to convert count data to activity, A (in mCi or MBq) or percent injected activity (PIA) or fractional injected activity (FIA = PIA/100) have been considered. One practical aspect of those methods is the use of a standard source (usually less than 1% of the injected activity in 10 ml) that can be placed in the camera field of view for every image. Test source count rates can be used to establish camera reproducibility over the course of the clinical trial. Total counts from the standard can also be used to assess possible dead-time correction factors for whole body and planar imaging.

Use of a well counter to measure blood, urine, and biopsy samples also requires standards that are a fixed fraction of the total radioactivity administered. Usually these standards are made up with a dilution factor of 10,000. In almost all cases, the well counter information is in concentration form: mCi/ml or MBq/ml. Estimation of the total amount of radioactivity in the blood or urine from well counter samples requires additional information. Frequently, plasma samples are collected and hematocrit values are required to extrapolate from plasma counts to whole blood concentration. Total urine volume would have to be recorded in the case of evaluating excreted activity.

B. Justifications for Data Modeling

A number of reasons exist for the generation of a mathematical biodistribution model. To first order in radiological physics, a model of animal or human data is required in estimation of absorbed radiation doses. This follows from the need to perform integration of normal organ and tumor activity curves out to many physical half-lives. By using only physical decay or some crude form of extrapolation from the last data point(s), the investigator is not effectively understanding the long-term course of the data. The same difficulty holds for estimation of activity values between data points as taken (i.e., the model also provides better interpolation).

A secondary reason for modeling, of more conceptual interest, is determination of rate constants and volumes descriptive of the tracer biodistributions. These parameters can be compared across different proteins and other agents to help in understanding the handling of the radiopharmaceutical *in vivo*. One of the most important of these parameters is the volume of distribution. Generally, these volumes are inverse functions of the molecular weight (MW) of a protein. Generally, as the MW decreases, the volume of distribution will increase.

Finally, there is the possibility that the model may point out that some data values are incorrect. Most such errors are due to mistakes made in the handling of information and not because of camera or other detector malfunction. These erroneous values will be far away from any model-generated functions and thereby noted by the investigator. In a data base analysis, such values must be screened out before the integrations to determine areas under the curve.

C. Types of Models

Two types of physiological model are in general use: simple curve fitting and compartmental analysis. We will describe the advantages and disadvantages of each approach. Both require the use of a computer-based algorithm to produce the best fit, usually via least-squares analyses, of a given set of model parameters. Goodness of fit may be judged by use of standard statistical parameters such as the correlation coefficient or R^2.

1. Individual Organ Curve Fitting via Multi-Exponential Functions

As the simpler alternative, one may consider a separate multi-exponential representation for each of the various blood, normal organ, and tumor curves. In this open model strategy, there is no explicit relationship between the various sets of exponentials from one organ to another as these fitting processes go on in isolation. This type of solution has certain justification since Laplace Transform analysis shows that linear compartmental modeling, as described below, leads to a set of linear differential equations whose solutions are indeed combinations of various exponential functions (Wagner 1975). In practice it may be difficult, however, to fit more than two exponential functions to any organ curve. For one thing, only a single exponential solution is unique. Solutions involving multiple exponential functions have different results depending upon starting conditions for the modeling algorithm used. This was the reason that single exponential fits were shown in the murine data analyses of Appendix A. Thus, complicated uptakes are not readily represented via this strategy. The PLOT software package, allowing up to three exponential functions, is available with MIRDOSE2 software from Oak Ridge Associated Universities (Watson et al. 1984).

2. *Compartmental Modeling of the Entire Physiological System*

The general motivation for compartmental modeling lies in the ability to fit **all** of the biodistribution data simultaneously. Given the model, one then has a representation that gives distribution volumes, rate constants, and other parameters. Some advantage in the understanding of the biodistribution may result from this more cohesive set of fitted parameters. Two general programs are presently available: SAAM and CONSAAM (Foster and Boston 1983) and ADAPT II (D'Argenio and Schumitzky 1979). Both are operable on a standard PC. SIMPLE, available from UCLA, runs on the Macintosh platform (Gambir et al. 1991).

Two general types of local relationships are found in closed compartmental analyses. These are the mammillary and catenary forms as given in Figure 5. Note that, for most agents, the injection of the labeled material into the blood implies that the vasculature will act as the source compartment for all other organs (i.e., the mammillary picture). This holds even for cases of intraperitoneal, intra-arterial or intralesional injection or even inhalation of radioactivity due to eventual appearance of the label in the blood compartment. Catenary (chain-like) features are found in the excretion or processing of the labeled material. Renal and gut excretion might be expected to exhibit this type of behavior. A given agent would probably show some of each of these patterns. Because much of the input data were acquired via imaging, blood may be used as part of any organ compartment. This assumption may be not be necessary in the case of animal biodistributions where blood has been removed from normal tissue and tumor samples before counting.

Two catenary subroutines are built into both MIRDOSE2 and MIRDOSE3 programs. One is used to describe the chain from blood to kidney to urinary bladder (Watson et al. 1984). The other describes excretion via the gut; small, upper large, and lower large intestines are included in that catenary picture. Readers should not, however, believe that their radiopharmaceutical will necessarily follow either of these two schema. Instead one needs to confirm that such simple processes actually describe elimination of proteins or their metabolic products. It may be more likely that a patients's gut excretion rather than renal excretion would be similar to that available in the MIRDOSE programs (Breitz et al. 1993). This follows from the possible interaction of fragmented antibodies within the renal tubules.

D. Which Data to Analyze

Modeling is done using organ biodistribution data presented as a function of time. Generally, a model's mathematical form would deal with an organ's uptake, not the organ's uptake per gram. This means A(activity/organ), as given as a series of time points, is the appropriate input information. Motion of material and the

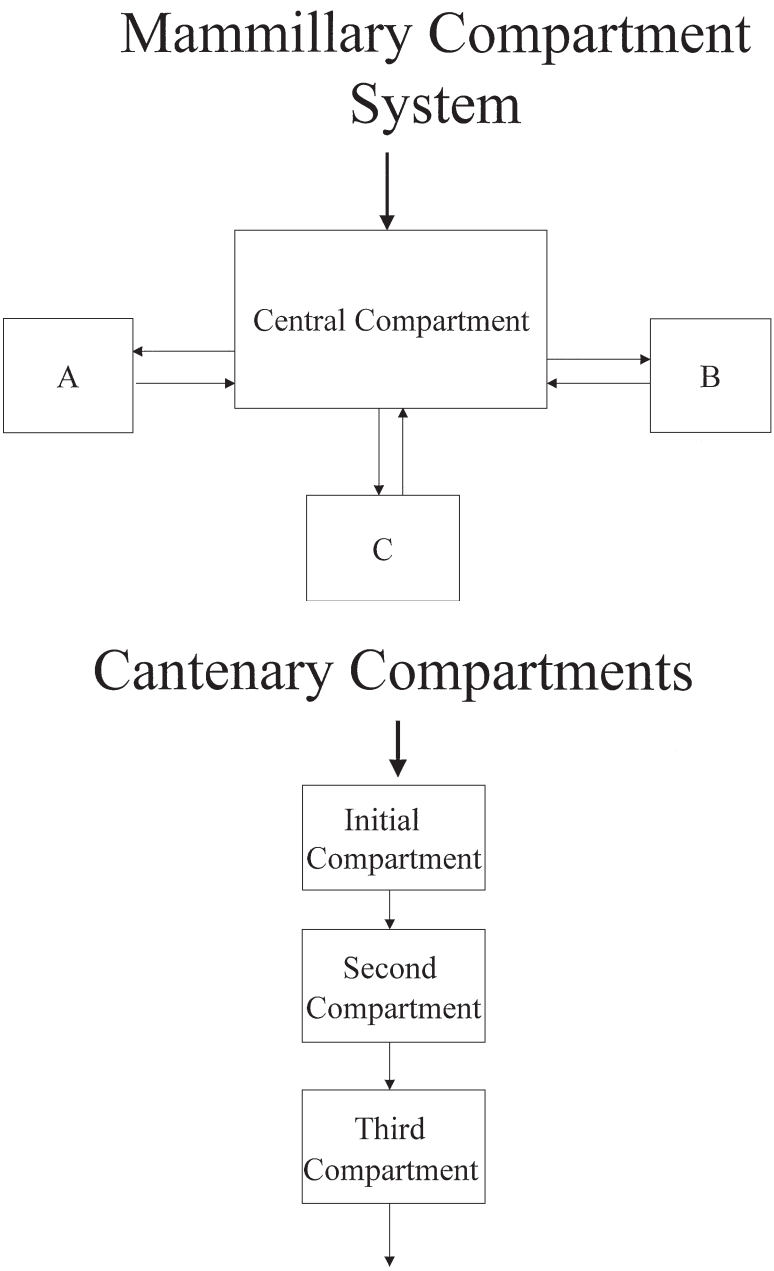

Figure 5. Mammillary and catenary model subsystems.

conservation of matter (activity) are readily accomplished with these variables. Data in the form of u(activity/gram) are usually not immediately appropriate since such specific uptakes are not directly relatable to the model variables. It may be possible to take the mathematical picture as derived for the A variables and recast it into the u variables by respectively dividing through by organ masses. In the case of clinical results, the last conversion may not be achievable, however, due to uncertainties in patient organ size.

This conversion is required, however, in the case of blood samples whereby the total volume of distribution is unknown—particularly for a novel protein or new tracer. In this case, the A variable for the blood is explicitly modeled as $u(\text{blood}) * V(\text{blood})$ where the latter volume is determined by the fitting algorithm. Note that u is the measured quantity in this case, not A.

E. Physical Decay as a Clearance Mechanism in the Model

Most literature biodistribution data have been corrected for physical decay so that the given percent injected dose/organ (PID/organ) or PID/g value is that of an associated hypothetical pharmaceutical—**not** that of the decaying radiopharmaceutical. If the analyst is interested only in pharmacokinetics results and the model is of the linear type, such data may be taken directly into the modeling equations. Rate constants, volumes, and other parameters will then be appropriate for the decay-independent model.

In the case of radiological physics, however, such decay-corrected data are not appropriate for analyses prior to Medical Internal Radiation Dose (MIRD)-type absorbed dose estimations (Snyder et al. 1975). This follows from the fact that the user is interested in finding an area under the organ's curve of activity versus time. These integrals are the total number of decays in the various source organs within the patient. Thus, the user may prefer to go back to the original data to find the appropriate inputs into the modeling program. Alternatively, one may simply multiply decay-corrected data by $\exp(-\lambda t)$ in order to take out the decay corrections the author has placed in published reports. Here, λ is the physical decay constant in units of inverse time. Some statistical impact is expected in such cases as measured data will have fewer counts at long times as compared to the decay-corrected published data. Notice that the model must, in this case of dealing with decay-containing data, include the physical decay as an output from each compartment. If the model is non-linear and/or non-homogeneous, however, the modeler must be careful to substitute the true data (uncorrected) into the equations. The latter must themselves contain physical decay as an explicit route out of each compartment (Williams et al. 1995b). In this case, one cannot simply correct the data for decay; the decay must be included in the model *a priori* or else incorrect results may appear in the solutions.

F. Integration of Area Under the Curve (AUC)

1. Mathematical Form

Some users prefer to estimate activity integrals under PIA versus time curves with a simple trapezoidal or other rule (Chaney and Kinkaid 1985). Usually, the region of the curve beyond the last measured point is represented as a single exponential based on the effective half time calculated from the last 2 or 3 points. This is still a model—albeit one without a physical basis. The accuracy of the AUC will depend mostly on the magnitude of the last point relative to the maximum values for each uptake site.

A purely mathematical form of integration has another application in dose estimation in a modeling context. It may be the case that one organ system, such as the kidneys, is only imaged in a relatively small subset of the patients. Thus, due to a lack of renal data, the model cannot contain a kidney compartment. For those patients whose renal system is imaged, the user may prefer to perform that particular integration via a trapezoidal or other mathematical rule as a separate procedure.

2. Multiple Exponential Functions

Integration of the open model or multiple exponential picture of organ activity is performed analytically using the fact that the integral of $a_i \exp(-k_i t)$ from $t = 0$ to ∞ is simply a_i/k_i. Thus the sum of such exponentials becomes a sum over the amplitudes (a_i) of each term divided by the relevant rate constant (k_i).

$$AUC = \sum_{i=1,n} \left[\frac{a}{k} \right]_i \tag{17}$$

It is useful to recall that the physical decay constant is generally implicitly part of the k parameters. Any given k can then be represented as $k_b + \lambda$ with k_b being the biological clearance constant.

3. Compartmental Model

In either the ADAPT (D'Argenio and Schumitzky 1979) or SAAM (Foster and Boston 1983) programs, integration of the time-activity curves is accomplished by defining a mathematical compartment as the integral of the organ compartment of interest. For example, if we set the activity in compartment one equal to A(1), then its integral is:

$$\tilde{A}(1) = \int_{t=0}^{\infty} A(1)\, dt \tag{18}$$

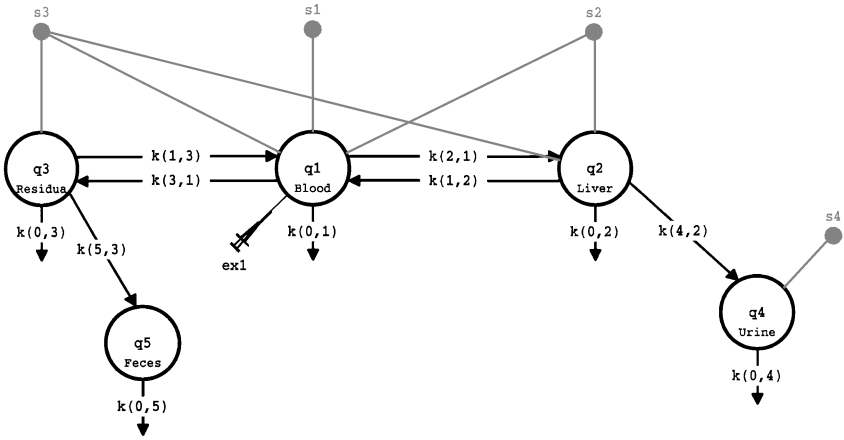

Figure 6. Five-compartment model for the intact antibody cT84.66.

Here, $\tilde{A}(1)$ is formally the time integral of compartment one. Notice that $\tilde{A}(1)$ is not sampled, and can only be computed using the fitted organ one activity curve. With ADAPT, this computation may require extensive processor time due to the step-by-step integration necessary in a modeling program. Convergence may also be questioned and is best answered by looking at the graph of $\tilde{A}(1)$ as a function of time. If the integral converges, this function approaches a constant value. An integration compartment must be defined for each of the modeled physiological systems. Thus, if 5 organs are modeled, 5 equations of the form given above will need to be added to the analysis. In this case, a total of 10 differential equations will have to be solved simultaneously. One may consider this complexity to be a disadvantage of the modeling approach as compared to a purely mathematical integration. This last consideration is a reason for multi-exponential representation of an organ's activity data. Figure 6 contains the five compartment model used to represent the antibody cT84.66.

Uncertainties in the integrals are generally not discussed by investigators. One method to estimate the errors in the AUCs is to use the covariance matrix available from the fitting procedure. This matrix, with Monte Carlo methods, will allow simultaneous prediction of the variation of areas for each of the organ compartments (Kaplan et al. 1997). While this type of analysis may be performed separately on each of the organs in an open compartment analysis, that result will tend to misrepresent the variation of AUC since the cross-correlations are not included in the process.

Given the $\tilde{A}$, the user must substitute this set of values into the fundamental MIRD formula of eq. (1). Generally, one retains the units as taken, μCi − h or decays, for this computation. The resultant dose is then in rads or cGy if the S

matrix value is in appropriate units. If one wishes to compare various patients with each other or with animal studies, the computation is in rad/μCi or cGy/MBq injected activity so that residence times (τ) are used in lieu of $\tilde{A}$ in eq. (1).

4. Variation of the Radionuclide

It may occur that the imaging radionuclide must, of necessity, be different from the therapy radionuclide. One example of this sort is the use of the ^{111}In-labeled protein as imaging tracer for the ^{90}Y-labeled protein. Organ activity information, obtained via the photons emitted by the imaging label, must then be recast into activity appropriate for the therapy agent. This is conventionally done by simply changing the physical decay constant in the modeling equations. Whether the user has an open model or compartmental picture, the decay constant of the therapy radionuclide is entered in lieu of that of the imaging radionuclide.

VI. DOSE CALCULATION METHODS AND PROGRAMS

A. Normal Organ Dose Estimates in Standard Man

1. MIRD 11 Pamphlet S Values

As a first choice in normal organ dose estimation, the user may elect to multiply the cumulated activity $\tilde{A}$ value set by a standard tabulated S matrix. The MIRD 11 Pamphlet, published by the Society of Nuclear Medicine is probably the best-known source of these values (Snyder et al. 1975). Radionuclides available include ^{131}I, ^{90}Y, and ^{111}In. In the pamphlet, both penetrating and non-penetrating radiation S values are summed to provide a net S matrix. It will be found that so-called pure beta emitters such as ^{90}Y and ^{32}P are diagonal matrices (i.e., Bremsstrahlung radiation is not included in these Monte Carlo S values). A method to include Bremsstrahlung radiation dose is described in section VI.C.5.

The Monte Carlo S matrix computation done in the MIRD Pamphlet 11 tabulation was performed using a computer-based set of humanoid phantoms. Uniform distribution of radioactivity in the source organs was also assumed in this approach. It is important to understand that these phantoms do not exist as physical objects; instead they are mathematical intersections of various geometric solids which simulate shape and position of a given organ system. For example, the thyroid is a set of tangent ellipsoids and the bladder is a sphere. Absolute size of these intersections is determined by standard organ masses available from physiological data sets. Because of these standard geometric shapes and locations, the MIRD phantom set is most appropriate for a dose estimate involving legal questions and theoretical consequences. An example is an Investigational New Drug

(IND) Application sent to the FDA. We have previously discussed using animal biodistribution data as an input to this type of computation.

Reviewers of the IND application are generally not interested in a specific patient's absorbed dose estimate. Instead, they want to find out how the applicant's dose estimation for a novel radiopharmaceutical compares to other, similar agents. By using a standard set of *S* values, the applicant allows the FDA to follow its computations more readily than if a patient-specific dose estimate were made. We will describe individualized absorbed dose estimates in section VI.B.

2. MIRDOSE2 and MIRDOSE3

A more efficient method for selecting S values is the use of either of the two standard programs available from Oak Ridge Associated Universities (ORAU). These S values are generated in real time using a parameterization of the MIRD Pamphlet 11 values for a given radionuclide. The older of these, MIRDOSE2, is available as a BASIC program which runs using the BASIC interpreter on a PC system (Watson et al. 1984). Source code is available which the user may examine and change as needed. For example, one could add a subroutine to supply an organ system model to describe the clearance of the radiopharmaceutical. PLOT, a three-exponential fitting algorithm, in BASIC, comes with the program. Catenary models of renal and gut excretion are part of this package. Figure 7 contains a summary of the steps required in the estimation of normal organ doses.

In 1996, an updated version, termed MIRDOSE3, was made available from ORAU (Stabin 1996). MIRDOSE3 runs under WINDOWS 3.1 with an icon system of choices. These include radionuclide and phantom selection. One can also print the S matrix of interest to accompany the dose estimation report. Unfortunately, the PLOT software is no longer part of the package so that the modeling aspects must be done externally. The catenary models for renal and gut excretion are included however.

One difficulty in using MIRD Pamphlet 11 is the lack of a "remainder of the body" as a possible source organ in the tabulated S matrices. One cannot use the total body term as that Monte Carlo estimate assumed that the activity was uniformly distributed in the total body of the phantom (Loevinger et al. 1991). The remainder of the body is the difference between the total body and the organs that show individual uptake. Thus, it is a variable source organ. The MIRDOSE3 program allows direct input of the remainder of the body residence time so as to eliminate this problem.

A total of six phantoms are available with MIRDOSE3. These range from fetus to adult male- and female-sized individuals. Since a typical RIT protocol will only involve patients over the age of 18, it is unlikely that this selection range will be required in a treatment plan. There is, of course, the possibility that if a patient is unusually small, then the 15-year old or even younger phantom might

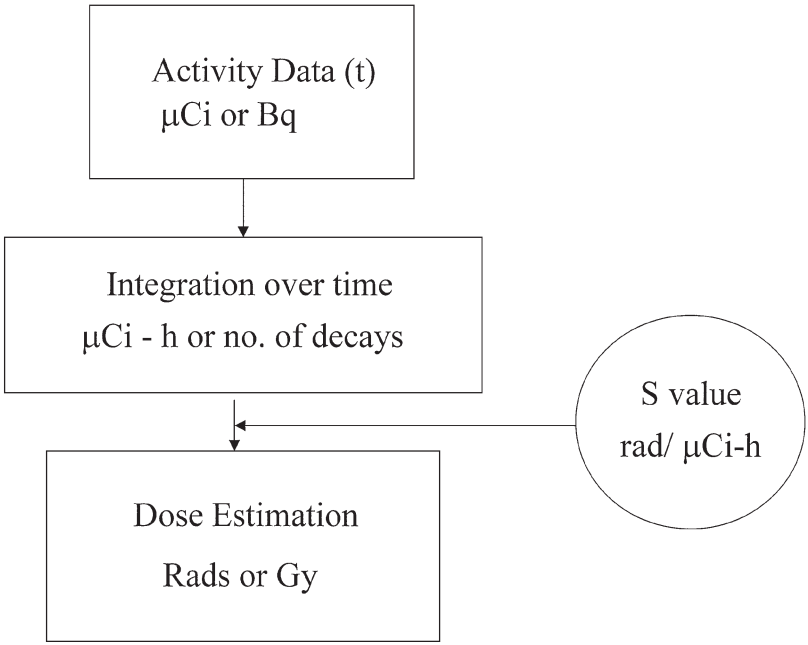

Figure 7. Outline of the general dose estimation process.

be of interest. A sample absorbed dose estimate for the adult male phantom using the geometric mean method for uptake measurement is given in Appendix C. Integration of the activity curves was done with the five-compartment model of Figure 6.

3. Bone Marrow Dose Estimation

Because of the enhanced radiosensitivity of the blood-forming cells, the red marrow is frequently the dose-limiting organ in RIT. The sensitivity of the red marrow to ionizing radiation is limited to about 500 rads for external beam radiation and about 200 rads for internal emitters. Most RIT treatment plans consequently rely on providing the best estimates for red marrow dose based on a range of assumptions and uncertainties. Frequently, patients enrolled in RIT protocols have undergone other therapies which may have damaged a large fraction of their marrow reservoirs. The marrow mass and distribution in these patients may be uncertain and the mass correction factor will be unreliable—albeit greater than one since the residual marrow mass is likely to be less than the value assumed in MIRD Pamphlet 11.

Three source organs are generally assumed for estimating marrow dose in RIT. These include activities in the marrow, bone, and residual body. This can be expressed as:

$$D_{rm} = D_{rm \leftarrow rm} + D_{rm \leftarrow bone} + D_{rm \leftarrow RB} \tag{19}$$

Radionuclide organ imaging methods often cannot separate these three source organs and sometimes a biopsy sample may be useful. Counts from an iliac crest or other bone marrow sample may be used to normalize to imaging data taken from the gamma camera (Macey et al. 1995). Such samples, however, only represent a single determination (snapshot) of a radioactivity distribution that is changing and repeated samples are not easy to procure because of the trauma to the patient.

If the radiolabeled antibody is assumed to be localized uniformly in the red marrow, an aliquot can be used to provide estimates for total marrow uptake based on imaging a small region of the marrow. A first order approach to providing estimates of specific marrow uptake has been attempted based on the ROI counts detected in the sacrum or 3 lumbar vertebrae (Macey et al. 1988). Integration of the uptake curves obtained over any of these areas is used to provide an estimate for specific uptake in total marrow. If little or no net activity can be visualized in these regions, an alternative strategy must be used. Generally, this involves the blood curve of the patient.

It has become more generally accepted that, in the case of marrow dose estimation, one can use the blood concentration curve as a surrogate for the marrow concentration curve (Siegel et al. 1990). Instead of a direct correspondence, the marrow $\tilde{A}$ value is set equal to a fraction (f) of the blood curves $\tilde{A}$:

$$\tilde{A}_{rm \leftarrow rm} = f\tilde{A}_{blood}\left[\frac{1500}{5000}\right] \tag{20}$$

where 5000 (g) refers to the whole blood mass and 1500 (g) the normal red marrow mass in the adult. Physically, this relationship is an attempt to correct, to lowest order, for the mass difference between the whole blood and red marrow. Values for the *f* factor have been estimated to lie between 0.2 and 0.4; a most probable value of 0.34 to 0.36 has been determined by Sgouros (1993). Note that this is only one term in the estimation of $\tilde{A}$. Two other terms arise from specific uptake in the bone itself and from radioactivity in the remainder of the body. Figure 8 summarizes the steps required to estimate marrow dose. Appendix D demonstrates a bone marrow dose estimation using the technique of eq. (20) and a residual body source term.

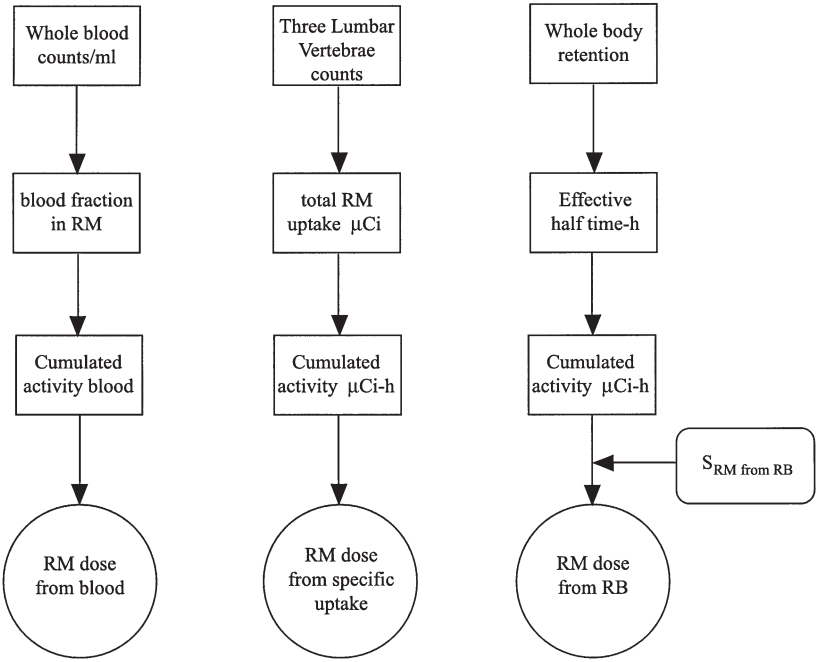

Figure 8. Schematic of red marrow dose estimation.

B. Patient-Specific Normal Organ Doses

1. Target Organ Mass Correction

One cannot assume that a given patient is exactly the size prescribed by one of the MIRDOSE3 phantoms. As was noted in section III, a CT scan is generally done before RIT in order that the medical oncologist has a baseline measurement of tumor sizes and locations. As a side benefit, this scan, or perhaps a comparable set of MRI images, can be spatially integrated to provide true organ sizes. Given this size, one may correct the MIRDOSE3 or other normal organ S value by simply scaling a mass correction factor for the non-penetrating (np) contribution. Let us consider a sample patient-specific computation using MIRD Pamphlet 11 tables of S matrices and breaking the value down into its penetrating (p) and non-penetrating (np) components:

$$S_p = S_{MIRD11} - S_{np} \tag{21}$$

As an illustration of this simple mass correction approach, suppose the mass of the spleen in a patient is known to be enlarged by a factor of 2 compared with the MIRD Pamphlet 11 phantom model of 173.6 g. For ^{131}I in this spleen, the S_p value will be given by:

$$S_p^{spleen} = 0.0026 - \frac{0.408}{173.6} = 0.00025 \tag{22}$$

where the np component has been calculated using eq. (2) and the emission data for ^{131}I. We have written this term purposely as a ratio of the numerator of eq. (2) divided by the MIRD phantom splenic mass. For the enlarged spleen the first order corrected S value will be:

$$S_{(347g)}^{spleen} = \frac{0.408}{347} + 0.00025 = 0.00143 \tag{23}$$

For the 347 g spleen, the S_p value for ^{131}I could be more accurately derived by interpolating the change in absorbed fraction with mass for the range of photons emitted, but since this changes slowly with mass, a first order estimate is accurate to better than 5% of the final value that would be returned. In our example, this simple correction for the S value reduced the absorbed dose to the spleen by 45%. The primary correction factor was the inverse dependence upon mass given in eq. (2). Anatomic information is essential to the method so that CT or MRI data will need to be available for the computation to proceed. A more complete description, including discussion of the gamma ray contribution which has been neglected here, is given by Shen et al. (1997).

Other methods may be used in lieu of the MIRD Committee and MIRDOSE approach. These techniques for individual doses are not based on Monte Carlo methods and mathematical phantoms. Instead, one uses the actual patient geometry given from the anatomical image set and explicitly calculates the absorbed dose to a voxel in the target organ space given a set of voxels of activity distributed in the patient's source organs. We will discuss two of these methods.

2. *Convolution Dose Estimates*

The most exact method for normal organ (or tumor) dose estimation follows from the use of a point source kernel or function (PSF) for a selected radionuclide in an infinite, unit density medium. These functions provide a look-up table for the dose rate as an isotropic function of distance between source and target. Tabulations are available for electron and photon energies commonly found in RIT (Leichner 1992). Previously, PSFs have been generated for monoenergetic electrons (Berger 1971). The PSF for a radionuclide is the sum of the dose rate from each particle and photon emitted. The differential dose at a position y with a point

source at x is given the convolution:

$$\Delta D(y) = \Delta\tilde{A}(x) \otimes PSF(y - x) \tag{24}$$

where $\Delta\tilde{A}(x)$ is the differential cumulated activity at point *x*. This technique is entirely independent of S matrices but requires exact knowledge of patient anatomy and activity distribution.

The execution time required for the integration of this equation is the greatest obstacle to the method. For beta radiation, the only target usually considered is the source organ itself so that the integral is carried out rapidly. For photon doses, however, all possible sources must be included in the integration step. Consequently, implementation of the equation also requires information on the distribution of $\tilde{A}$ in each voxel; this may be difficult to determine in a patient. Such constraints force many users to assume uniform uptake as was done in providing MIRD Pamphlet 11 S results and the MIRDOSE programs. In spite of this, the actual spatial volume of the organ is being considered in the estimation so that the process is inherently superior to use of a precalculated S matrix.

One limitation of the point source method is that the medium is assumed to be uniform and infinite in extent. Usually a soft tissue framework is assumed. Hence, if there is significant variation in tissue type between source and target, the point source method may be significantly in error. This would not be the case within a soft tissue such as liver or spleen, but could occur near transition points such as bone structures or estimating dose to lung from sources in the liver.

3. Voxel Source Kernel Method

One strategy that is useful in patient-specific dose estimation is the generation of a small scale S value (i.e., one computed on a voxel basis). Here, the voxel would be one appropriate for the nuclear image being used for the uptake measurements (Liu et al. 1998). Any smaller scale S cannot be justified since the nuclear data do not have the requisite spatial resolution. Monte Carlo methods are used in the development of such voxel source kernels (VSKs). Dose estimates are then computed using a convolution approach, as in eq. (24), using the actual anatomic volume of the patient organ(s). These computations may also be performed on tumor sites and lymph nodes. A recent MIRD publication gives several VSK S values for a number of radionuclides of interest (Bolch et al. 1999).

C. Tumor Dose Estimations in Radioimmunotherapy and Radionuclide Therapy

In principle, there are three types of emission that may be considered in tumor dose estimates. Of primary interest are alpha and beta rays, which have a relatively short range and hence are localized in the lesion(s). Photon doses are usually of

secondary significance. In a practical sense, the most important non-penetrating radiation is the beta ray.

1. Alpha and Auger Emissions

Application of alpha particles has been difficult due to their extremely short range (10 to 100 μm) in soft tissue. Because antibody deposition is rarely within this distance of solid tumor cell nuclei, one has the possibility of ineffectiveness of such therapy. Exceptions can take place because of the movement of the antibody-antigen complex within the tumor cell. Additionally, there have been applications to leukemia patients wherein malignant cells are freely circulating in the blood. In either of those cases, the estimates must be done on a microscopic basis. In fact, alpha dose estimation is generally a microdosimetric method that requires exquisite geometric knowledge of radionuclide deposition. Such knowledge probably requires autoradiographic methods, which are difficult to use clinically.

A similar argument holds for Auger electrons emitted due to vacancies in atomic shells. These particles have ranges on the order of 10 µm at 20 keV. If the antibody radiolabel will be taken into the cell, preferably into the nucleus, such emissions may be considered for RIT. Otherwise, their application to therapy is limited. For these reasons, we will not consider alpha-emitters or Auger electrons in the following.

2. Beta Emissions

a. Uniform Uptake

Because of its essentially random location and size, tumor cannot be a source or target organ in the standard MIRD phantom format. There is, within MIRDOSE3, a separate algorithm which estimates beta doses to spherical tumors of a given size and having uniform uptake of the radioagent. Here, one supplies the tumor mass, the radionuclide, and an Ã value for this computation. Edge effects are explicitly taken into account (Buras et al. 1994). Doses due to other organs, however, are not included in the computation. Such effects are probably not significant for relatively large tumors. There may be, however, significant cross talk of high-energy betas from a nearby normal organ to the tumor (e.g., from the liver to a liver metastasis). A VSK may be used in this analysis as indicated in section VI.B.3.

b. Non-Uniform Uptake

Let us next consider the most general case of a non-uniform distribution of beta activity in the tumor and energy deposition that is non-local. The latter assumption follows from the extensive range of beta rays from radionuclides such as ^{90}Y (1.1 cm in soft tissue). Howell et al. (1989) have given S factors for various spherical tumor sizes and different non-uniform radionuclide distributions. In this case

one could directly substitute the resultant S into the general MIRD formula if the Ã is known. Thus, an S value does not necessarily imply uniform uptake within the lesion. The VSK approach, as described above, will also provide dose estimates for non-uniform uptakes by generating a voxel-sized *S* matrix. In any event, estimation will be separated into its two classical aspects: the evaluation of Ã and the determination of an S value or equivalent for the tumor geometry (Loevinger and Berman 1976, Loevinger et al. 1991).

3. The Tumor Ã Algorithm

Activity information may be obtained from an associated gamma emitter that has an identical or similar biodistribution in the patient. For example, if ^{131}I is the antibody radiolabel, the gamma rays from radioiodine point out the position of the radioactive atoms that are also a source of the beta radiation. Alternatively, one may use the ^{111}In-antibody in lieu of the ^{90}Y-antibody to establish the biodistribution *if* the labeling type does not affect the actual targeting *in vivo*. In practice, this method is less certain since no chelator is equally effective as one changes the radius of the radioactive ion. Finally, if a pure high-energy beta-labeled antibody is injected, one might use the Bremsstrahlung radiation images to quantify activity as a function of time in the tumor. In this case, however, the image quality is often poor unless one injects directly into the lesion (Siegel et al. 1994).

Using any of the above three strategies of following tumor radionuclide deposition, serial nuclear medicine images provide the data to be modeled for Ã evaluation. If one wants some idea of the heterogeneity of activity in the lesion, SPECT imaging may be the only possible modality. Otherwise, a ROI is drawn around a planar image of the tumor to delineate the pixels of interest and the activity as a function of time. Notice that the gamma camera image must be corrected for attenuation and scatter and be calibrated so that counts per minute or per image can be translated into μCi or MBq in the lesion. These methods are described in section IV.

4. Tumor Mass Determination

Tumor mass must generally be determined by some imaging method since external measurement or palpation is unlikely to be accurate for lesions within the patient. One exception to this rule may be Na^{131}I therapy of the thyroid, which is discussed below. Thus, CT, MRI, ultrasound or even planar X-ray images are preferable. If several dimensions are available, the physicist may represent the lesion as an ellipsoid with minor axes equal to half of each of the respective three dimensions. A lesion with two dimensions may be idealized as an ellipsoid of rotation. Likewise, if only one length is observed, the tumor may be represented as a sphere whose diameter is equal to that distance. Unit density is generally assumed in any case. Eq. (16) may be used in these computations.

Because of a lack of other information, it could be necessary to use the nuclear image to provide tumor geometry. If this is done, the resultant volume may be either larger or smaller than that found with anatomical imaging or at surgery. The former case of increased size occurs due to the scatter of the photons in the patient before reaching the detector. Some of this scatter is in the collimation system. As described in section IV, corrections to the nuclear image can be made by merging the CT and nuclear images so as to better define the actual lesion volume. Additionally, one may draw a satellite ROI near the source organ. Using count density from this background region, one may subtract counts from the source organ so as to get a better idea of the actual decay events therein. To a major degree, this is a correction for over- and under-lying activities.

The nuclear image may be smaller than the anatomical due to lack of perfusion of certain regions of the neoplasm. In this case, a dose estimate based on nuclear volumes may be too high and not appropriate for the tumor in question. If available, a comparison of nuclear image and non-nuclear image lesion dimensions may be informative. Overlaying images from the two modalities can help establish zones of poor perfusion and/or incomplete targeting. This last feature may also occur due to the heterogeneous expression of the antigen.

5. Computational Algorithms

If the activity distribution is heterogeneous and known, a direct Monte Carlo approach is one way to estimate absorbed dose in different regions of the tumor. Several programs are available including EGS4 (Ford and Nelson 1978), MCNP (Briesmeister 1993), and ETRAN (Berger and Seltzer 1973). Some of these codes, including MCNP, are available on PC computers. Geometric volumes allowed by these programs are limited, however, so that the true geometry of the lesion and its surroundings may not be acceptable as an input set of tally spaces. Computer time can be quite extensive and this sort of solution may not, therefore, be practical on a routine basis.

An additional approach to this general problem is to use a convolution method based on point source functions for the beta emitter of interest (Loevinger et al. 1956). Here, the estimated dose at the position y is given by the result of eq. (24). By means of Fast Fourier Transform (FFT) algorithms, this computation can be done relatively quickly for a simple tumor shape (Brigham 1974). The Fourier transform maps the convolution into a simple product of functions in the frequency (cm^{-1}) domain. Roberson and co-workers (1994) have performed extensive FFT calculations of this type in variously shaped human xenografts in a nude mouse model using autoradiographic data for the activity distribution $\tilde{A}(x)$. Alternatively, one may perform the integral of eq. (24) directly in the spatial domain. In this case, the time required may be prohibitive when the lesion has a random shape.

Finally, for high-energy beta emitters, there is the Bremsstrahlung radiation contribution (Williams et al. 1989, Stabin et al. 1994). This effect is rather small, on the order of one percent or less, unless the lesion lies within the normal organ (e.g., the gut for a colorectal cancer). A point source function is available for this effect in the case of ^{90}Y (Stabin et al. 1994). Given this function, convolution techniques as outlined above may prove effective in rapid computations for simple geometries. With a voxel source kernel, the Bremsstrahlung radiation can be explicitly included within the S matrix (Liu et al. 1998).

6. Photon Contributions to Tumor Dose Estimates

Both Ã and organ mass may be determined as described above. If the activity distribution and geometry are relatively simple (e.g., uniform uptake in a spherical tumor), one can find tabulated absorbed fractions appropriate to the photon energy. Such S values allow direct, rapid estimation of tumor-to-tumor doses. Even in such a simple case, the estimates of photon doses to tumors from other organs is difficult due to the random location of the lesion within the standard human MIRD geometry. One solution to this problem is to use a normal organ in lieu of the tumor to provide an approximate S value for the photon(s) of interest. A similar replacement strategy can be used to provide an estimate of normal organ target dose from a source within the tumor. Such replacements are sometimes called analogue source or target organs. If no normal organs of appropriate size and location are available, the whole body could be used in lieu of the tumor as a target organ; this is clearly an overestimate of the tumor-subtended solid angle. Resultant estimates will probably be too large and can only serve as an upper bound to the gamma-induced absorbed dose.

If we consider the most general case of heterogeneous activity distribution that is known, we can estimate absorbed fractions most generally with Monte-Carlo methods. Limitations are, as mentioned, due to the time required. Parallel processing has been advocated to permit more rapid estimates for a given number of photon histories (Johnson 1988). Convolution or direct integration over the source volume(s) may also be performed. Leichner (1992) has published point source functions for various monoenergetic photons. These two methods explicitly permit dose estimates to normal organs just as in the case of the beta radiation. As in that case, however, the computational time required may not permit practical clinical operation.

A probable better approach to the above situation is to use the MABDOSE program developed by Johnson and associates (Johnson 1988). Here, the gamma-derived absorbed dose estimates can be made for spherical tumors at various locations within the MIRD standard phantom geometries. Three Cartesian coordinates of the center of this sphere must be specified to begin the Monte Carlo based estimation process. Photon-derived doses to the tumor from activity both

within and without the lesion are included in the estimation. This program, running under Windows 3.1, is available on a PC.

7. Clinical Computations (Beta and Photon Contributions Combined)

All radionuclides, in practice, produce both particulate and photon emissions. Internal conversion and Auger electrons are seen, for example, in purely photon transitions. Likewise, pure beta emitters give rise to Bremsstrahlung radiation because of the presence of local tissue surrounding the emitter. Thus, the physicist will need to sum over both types of emissions to produce a general absorbed dose estimate.

8. Doses to Tumors That Are Not Imaged

One of the reasons for antibody or other systemic therapy is that undetected tumors may also be irradiated during the course of the treatment. Small metastatic lesions, lymph node localizations, and even microscopic clusters of tumor cells are possible targets for a radiolabeled antibody. It has been observed in human xenografts in mice and in a limited number of human results that an inverse relationship usually exists between tumor uptake (u) in PID/g and the mass (m) of the lesion (Williams et al. 1988). This relationship is in the form of a power-law:

$$u(m) = a * m^b \tag{25}$$

where a and b are constants independent of m. The exponent b is typically in the range $-1.0 < b < -0.1$.

For example, for primary colorectal lesions in humans, $b = -0.362$ was measured (Williams et al. 1993). Thus, if the beta radiation does not escape the tumor volume, one anticipates improved radiation dose delivery as the lesion mass decreases. Eq. (25) can be used to predict uptake for one or more lesions seen only on CT or MRI scan. Here, we suppose that the a and b coefficients have been determined using animal or human data. Human uptakes of antibody tracers have been measured by taking surgical samples post systemic injection. Values of u, corrected for decay of the radionuclide, are generally in the range of 2 to 20% ID/kg at periods of time between 5 and 15 days post-injection (Williams et al. 1993). These magnitudes are consistent with the results with human xenografts in nude mice provided that one takes into account the species mass difference and the variation of antigen concentration between the xenograft and human wild-type tumors. Thus, analysis of a murine model does provide a good prediction of the human tumor uptake in a clinical setting. A summary of tumor dose estimation methods is given in Figure 9.

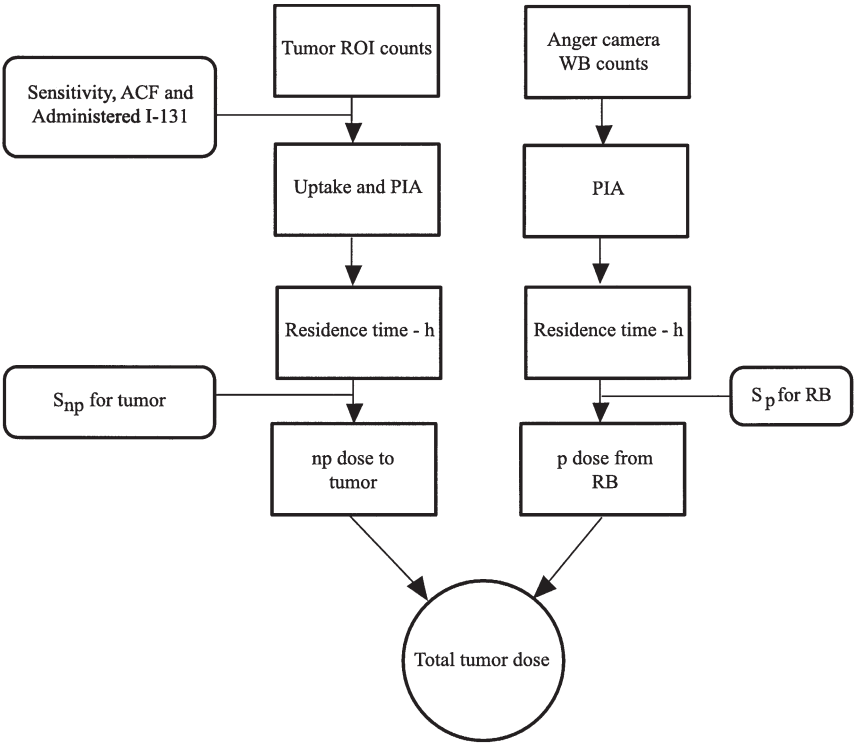

Figure 9. Steps in tumor dose estimation. ACF refers to attenuation correction factor.

9. Treatment Strategy and Results

It is often the case that red marrow toxicity is the activity-limiting step in RIT treatment planning. Although, for example, only weak correlations may be found between estimated marrow dose and the depletion of platelets, many patients exhibit a reduction of platelets with a nadir at approximately 4 weeks post-treatment (Figure 10). The likelihood that marrow effects will occur in a given patient depends upon the uncertain history of that individual's marrow depletion as a result of earlier therapies. Marrow storage is often used to preclude potentially fatal results. Figure 11 gives the overall strategy for treatment planning with a limiting estimated marrow dose of 200 rads or 2.00 Gy. If the projected dose exceeds this value, a reduction of injected activity or rejection of the RIT protocol are possible choices for the patient. Repeat RIT activities are generally the same as those used initially.

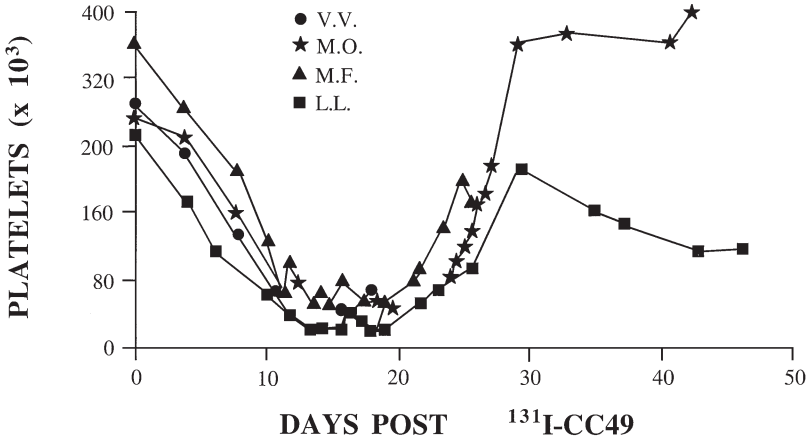

Figure 10. Typical platelet data from four representative ^{131}I-CC49 RIT patients.

VII. THYROID CANCER THERAPY - THYROID THERAPY WITH ^{131}I

The prototype for RIT is treatment of malignant thyroid disease with radioiodine. Here, there are three methods for estimating the amount of radioactivity to be given to treat the patient's remnant thyroid (Hurley and Becker 1983, Harbert 1987). These include a fixed small amount generally 30 mCi, a larger activity 75–150 mCi, or a calculated absorbed dose on the order of 3×10^4 rads (300 Gy) to the residual malignant tissue. Reasons for the 30 mCi protocol turn on the issue of patient isolation due to historical state and other regulations on radiation safety. These are discussed in section IX.

Some disagreement occurs as to the efficacy of a 30 mCi treatment strategy however, and that method would probably not be recommended generally (McCowen et al. 1976, Siddiqui et al. 1981). The most common treatment regimen is using a fixed activity of 75 to 150 mCi of ^{131}I with some authors claiming 85% success in achieving complete ablation—that is, no subsequent uptake of radioiodine in the neck area (Siddiqui et al. 1981).

If one uses a calculated absorbed dose value, calibration of the probe system usually relies on the counting of a known source in the same geometry as the patient. A neck phantom may be useful in this regard to simulate attenuation. Absolute uptake quantification has been developed using coincidence decays of gamma and X-rays from ^{123}I to evaluate the depth of the emitter in the neck (Siegel 1981).

If the physician elects to treat the patient by estimating absorbed dose, the activity-limiting organ has usually been the blood. Seen from the perspective of

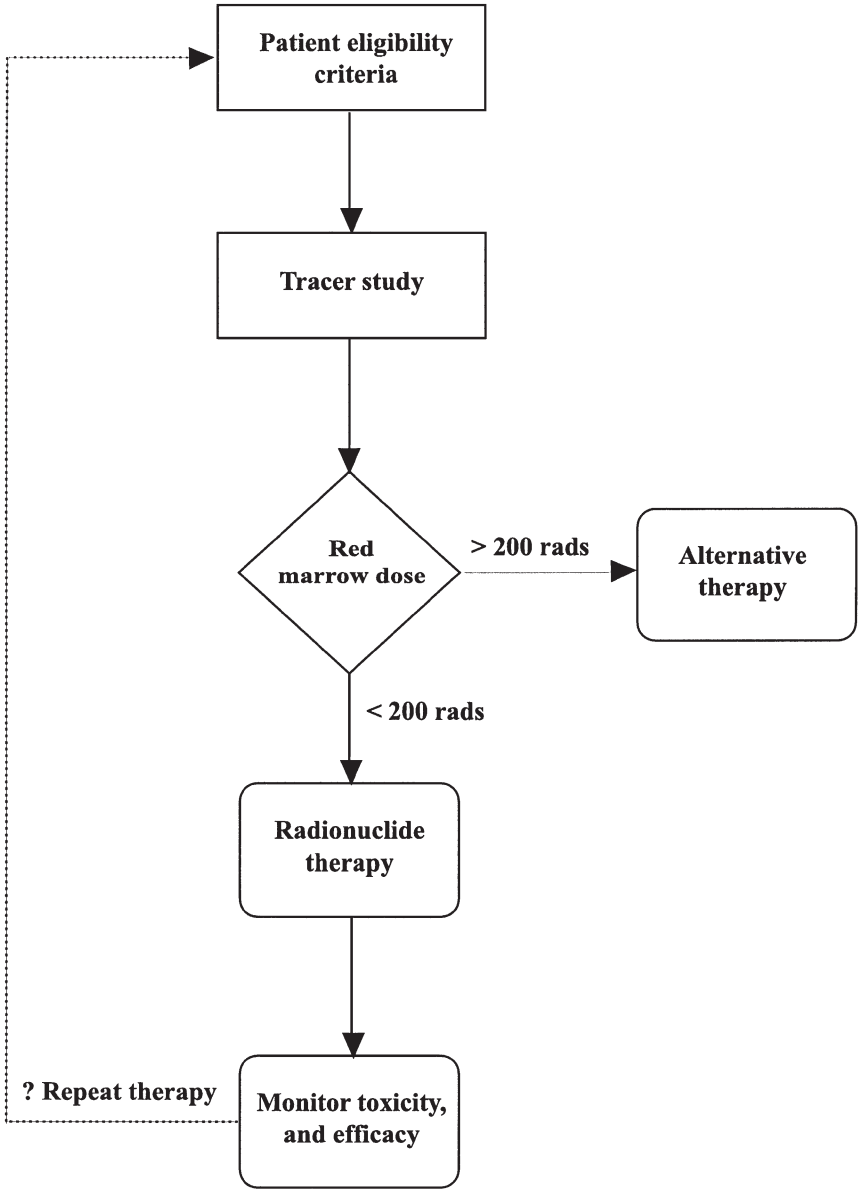

Figure 11. Treatment strategy for RIT based on limited dose (200 rad) to marrow.

RIT, this is very similar to the limitation due to red marrow dose. Generally, one attempts to keep estimated blood dose to 200 rads (2.0 Gy) or less. Since this treatment will follow surgical removal of the majority of the thyroid, the actual dose to remnant tissue remains uncertain, a difficulty that is also found in treating a small tumor of unknown size within the body of a patient using RIT.

As in the case of non-thyroid tumor therapy, the mass of residual thyroid tissue remains the primary uncertainty in the target organ absorbed dose estimation process. Both penetrating and non-penetrating radiation are included in the estimation. Possible radionuclides are ^{131}I and ^{125}I with advantages seen in the use of the former due to its greater beta ray penetration in soft tissue. It should be noted that use of ^{131}I may allow imaging of the biodistribution of activity during the course of treatment. Here, we assume rapid excretion of most of the activity after the first 24 hours so that the gamma camera is not overwhelmed with the count rate during therapy. Additional lesions may also be visualized using this high level of ^{131}I activity prescribed for the radiotherapy treatment. Thus, for most clinicians, ^{131}I is the radionuclide of choice in thyroid therapy. It is administered as the sodium salt—usually by mouth.

VIII. BONE PAIN PALLIATION WITH RADIOPHARMACEUTICALS

A. Clinical Situation

Prostate, breast, and other cancers may lead to multiple bone metastatic sites. While single sites may be treated with external beam therapy, multiple sites imply the use of a radioactive agent that can distribute as a bone seeker. In general, the treatment is not intended to reduce the metastatic site in size, but rather to induce a reduction in the patient's pain symptoms. The anatomic target of this radiation is not known. In several clinical studies, such palliation has been achieved at levels between 50% and 90% of the population. Pain may recur with subsequent treatment becoming necessary (Lewington 1996). Absorbed dose estimates have been made in only a minority of the clinical trials. Thus, it has not been possible to correlate the clinical outcome (i.e., the reduction of symptoms) with the estimated dose.

B. Radionuclides

A number of beta emitters, including ^{32}P, ^{89}Sr, ^{153}Sm, and ^{186}Re, have been investigated in these applications. Particulars regarding their beta (and possible gamma) emissions are described in Table 1. More recent trials have involved the last two radionuclides in the reduction of breast and prostate cancer bone pain. In

particular, ^{186}Re has chemical properties similar to ^{99m}Tc so that the latter tracer may be used to indicate the eventual biodistribution of rhenium. In this way, the physician may correlate the conventional bone scan image with that found during therapy (de Klerk et al. 1992). Presence of a gamma emission in the decay spectra of ^{153}Sm and ^{186}Re allows imaging of the distribution activity after injection of these radionuclides. In that way, the clinician can document uptake and, possibly, the reduction of a lesion's size.

C. Dose Estimation

Determination of activity within bone is probably the greatest obstacle to dose estimation using bone agents. Projection images may show accumulations that actually reflect uptake in hard bone, as well as trabecular bone and marrow. Thus, the clinician is usually limited to bone biopsy information. These data, however, are generally only obtained once for a given patient due to trauma and associated pain. It may be possible to correlate the biopsy with the image data, but this can be difficult.

Stabin and co-workers have used MIRDOSE2 and its ICRP 30 (International Commission on Radiation Protection and Measurements Report 30) subroutine to estimate marrow dose with ^{153}Sm bound to the chelator EDTMP (Eary et al. 1993). In that case, values of 5.7 rad/mCi administered activity were calculated. Since patients were treated with up to 3.0 mCi/kg, this led to red marrow absorbed doses of up to 2250 rad or 22.50 Gy. Yet only 2 of 4 patients experienced even mild hemotoxicity at this level. The authors comment that these doses were almost certainly overestimated due to the ICRP 30 assumption that all bone surfaces are in contact with marrow. Instead, the marrow is heterogeneously distributed within the bony matrix and has, particularly in the older patient, large amounts of yellow (fatty) marrow admixed within its assumed space inside the bone. In addition, many of these patients have been pretreated with various chemotherapy agents that may also have led to a change in their marrow mass.

A group at the University of Cincinnati has attempted to improve such bone marrow absorbed dose estimates using pathology samples and a Monte-Carlo approach (Samaratunga et al. 1995). They applied their method to ^{186}Re(Sn)-HEDP. In this case, S values were found to be considerably higher in the Monte-Carlo method than that found using a homogeneous model of the soft-tissue (lesion) distribution within the bone matrix. This work, entirely microscopic, did not attempt to compare its results with the traditional MIRD organ-sized analyses described in this report.

We would conclude that bone marrow dose estimation for bone-seeking radiopharmaceuticals is not a simple exercise (Bayouth et al. 1995). As indicated above, while new information is available on S matrix values, bone and marrow

biodistribution data are difficult to obtain. The latter result will probably not improve in the near term. It is therefore tempting to validate instead the computations (if any) of marrow absorbed dose with clinical blood chemistry post-therapy. This method will, at least, demonstrate a practical method for estimating red marrow absorbed dose. It may also be compared to external beam results.

IX. RADIATION PROTECTION CONSIDERATIONS

We have previously discussed protection of the patient by use of dose estimation techniques. We will now describe protection of personnel involved in preparing radiopharmaceuticals, caring for the patient, patient relatives, and the general public. In particular, nursing staff should receive training on caring for patients who have received radiolabeled antibodies and how to manage a spill of radioactive material. Specific precautions required during administration of the radiopharmaceutical have been described in section IIIC.

A. General Radiation Safety

The following guidelines, which are similar to those for patients receiving ^{131}I therapy, should be observed. Visitors must be at least 18 years old. Pregnant women are not permitted in the room. Patients should be confined to their rooms except for special medical procedures. Patient meals must be ordered on isolation trays and trays must remain in the room until checked by radiation safety personnel. The floor around the toilet must be covered with absorbent pads. A summary of these guidelines is given in Table 5.

To reduce exposure, nursing staff should spend a minimal amount of time in the room, i.e., only that required to administer satisfactory care to the patients. The radiation safety officer (RSO) or staff physicist should post the maximum time on the door. A personal dosimeter may be provided for hospital staff. In that case, a logbook is placed at the entrance to the patient area and dosimeter readings are recorded at the time of entrance and exit by each person entering. Shoe covers must be worn and placed in a designated container on leaving the room. When in the room, assume radioactivity is present in all bodily fluids and excretions. Observe universal precautions and wash hands well when leaving the room. Gloves are mandatory when drawing blood, handling urinals, bedpans, emesis basins or other containers having any materials from the patients. Gloves and sharps are to be disposed of in containers in the patient's room. The toilet should be flushed three times after use. If urine is to be collected, all urine collections should be handled over disposable pads. Any contamination on container surface should be wiped off. If urine is to be transferred, the container must be rinsed several times with hot soapy water.

Table 5. Radiation Safety Guidelines for Patients Receiving Radionuclide Therapy

- Admit patient to single room
- Cover floor near toilet with absorbent pads; use pads for any procedure where contamination is likely.
- Cover traffic areas with absorbent pads
- Cover door knobs, bed controls, and telephone handset with plastic wrap
- Confine patient to room except for special medical procedures
- Radiation placard on door
- Principles of time, distance, and shielding applied
- No visitors under 18 years of age.
- No pregnant visitors
- Universal precautions
- Assume all body fluids are radioactive
- Gloves and sharps disposed in container in patient's room
- Flush toilet three times after each usage
- Isolation trays used
- Contaminated non-disposable materials stored in isolation until decay (10 half-lives).
- Specimens leaving room monitored for contamination.
- No housekeeping until patient discharged and room cleared by RSO or Staff Physicist

B. Discharge of Patients with Radioactivity from Hospital

The RSO or staff physicist will determine when the patient is to be discharged. Regulations depend upon the local license stipulations, but will be within general guidelines specified by the controlling agency. For the Nuclear Regulatory Commission (NRC), these rules have changed recently and now may be related to the actual total effective dose (TEDE) to individuals in the patient's home environment (USNRC 1997). For the 20 states covered by the NRC, three alternative release criteria are possible. These are:

(1) documented activity in the patient,
(2) exposure rate at one meter from the patient or
(3) estimated TEDE value to patient family members.

In the last case, the limit is 0.5 rem and the estimation must be made on a patient-specific basis prior to release. In the case of the (1) or (2) criterion, the magnitude of the maximum activity or exposure rate value at time of release depends upon the radionuclide (USNRC 1997).

For agreement states, criteria may differ from the NRC values. For example, the previous federal rules permitted a maximum of 30 mCi of activity or 5 mR/h at one meter from the patient at the time of release. These values are still in force at many institutions. Zanzonico (1997) has shown that if hyperthyroid patients were released with a mean activity of 29 mCi, their family members received an average of 500 mrem. Both direct irradiation and radioiodine uptake were considered in these measurements which justified the older, more restrictive, regulations for non-malignant disease.

Patients with thyroid malignancies, given that they will initially undergo thyroidectomy, will demonstrate much more rapid clearance of the radioiodine and hence justify more liberal release criteria than that used for hyperthyroid patients. It is unlikely that RIT patients will show such rapid clearance. Dehalogenation of the radioiodine in a RIT protocol may allow more rapid excretion than with a radiometal label on the antibody, however. Whole body and various organ retentions of the antibody LYM-1 are given for a typical patient in Figure 12.

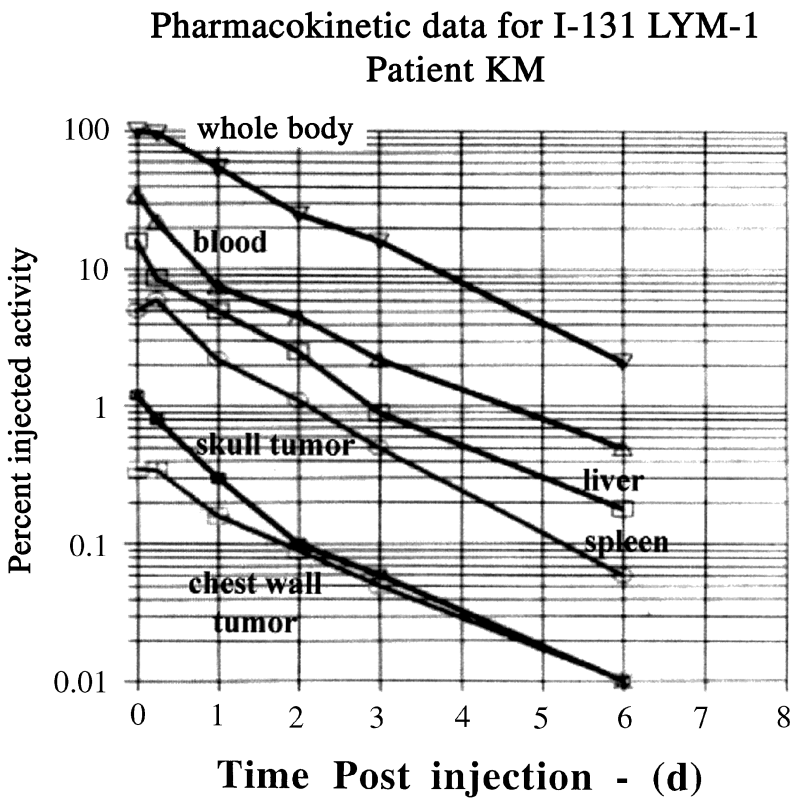

Figure 12. Whole body and organ retention data for a ^{131}I-LYM-1 patient.

When the patient is discharged, the room must be surveyed for contamination before it is released for use by others. This process involves both room surveys and the swabbing of surfaces to detect removable activity. Pure beta sources may be counted using either Bremsstrahlung or, if energetic enough, Cerenkov radiation. Calibration of the counter is provided by an aliquot of the injected activity.

X. SUMMARY OF RADIOIMMUNOTHERAPY AND RADIONUCLIDE THERAPY IN CLINICAL PRACTICE

A. Treatment Planning

RIT requires extensive staff involvement and equipment preparation. Nuclear Medicine personnel must acquire uptake information from the major organ systems and perform integrations out to times on the order of 10 physical half-lives. As we have seen, activity values in patients may be determined by one of several methods with uncertainties between ±10% and ±30%. Generally, the GM strategy has been the most commonly used with the requirement that two opposed images be determined at each time point in the study. Alternatively, quantitative SPECT or the CAMI method may be invoked if this condition is not met. Integration of activity is best done with a physiological model that includes all the imaged compartments as well as fluid samples. Errors in this process are probably on the order of ±2% to ±10%. Lastly, the provision of S values in the standard MIRD formula requires that the target organ or tumor mass be determined with anatomic imaging. If this is not possible, errors on the order of factors of two- or three-fold are not unexpected due to the differences between true organ sizes and the MIRD phantom values assumed (Liu et al. 1998).

Overall, one anticipates that **at best** the estimated absorbed dose in RIT trials is correct to within ±20%. This result is much worse than the value usually given for external beam therapy (±5%). Such comparisons are probably better done, however, by looking at dose-volume histograms whereby the differences may not be as striking. As the use of Monte Carlo methods increases, such histograms will become common and allow us to better visualize the estimated dose distributions provided by each modality.

B. Clinical RIT Results

At present, only two commercial RIT trials, both involving treatment of B-cell lymphoma, have been initiated. A large number of local Phase I and Phase I/II protocols are underway for the treatment of blood diseases and solid tumors. While lymphomas have shown good response to RIT, little progress has been seen with solid lesions. This result is viewed by some as being consistent with the ineffectiveness seen with external beam therapy of the same diseases (e.g., colon cancer). Use of

RIT in the adjuvant setting is not yet in any widespread use. As we noted in section VI.C.8, the smaller tumors are better targets for radiation therapy using internal emitters. One can expect more RIT protocols following surgical removal of the primary disease site(s). This application may eventually become their primary clinical use.

In the near term, one can anticipate that the number of trials will continue to grow as more antibodies and their fragments are engineered. Certain applications, such as the purging of diseased marrow using labeled antibodies, will increase and may eventually supplant external beam treatments. It is possible that RIT will evolve as a preferred modality for lymphoma therapy. The sensitivity of this disease to ionizing radiation and the localization of the absorbed dose derived from RIT are the primary reasons for this prediction.

Patient-specific absorbed dose estimates will become necessary to understand the effectiveness of all trials. While MIRD-type estimates will still be made for the FDA, one expects the specific dose estimate, or treatment plan, will become much more common. Such absorbed dose values will then be compared with the tumor effects and normal organ toxicities observed in the clinic. Here, one may find that the rad or grey dose estimated via a patient-specific calculation is not directly comparable to external beam doses delivered over much shorter times with extended rest intervals between treatments.

We also expect that there will be some effort to add radiation sensitizers to the treatment regimen. Presumably given prior to RIT, these agents could lead to greater cancer cell sensitivity to the beta (or alpha) radiation involved in the therapy. In such work, the importance of physiological models will become much more significant than we have indicated. Using such models and knowledge of the cell cycle, one could hope to optimize the treatment of a given solid tumor.

C. Limitations of the RIT Method

Since the cancer patient can never be assumed permanently cured, ongoing therapy is a requisite for any treatment system. At present, the appearance of patient-derived antibodies to any administered protein may be the greatest limitation to the RIT strategy. Engineering work on the design of these proteins is continuing, however, and will result in improved agents that elicit lower responses from the patient's immune system. In this work, the human backbone structure will be included with initially an animal-derived recognition site. Eventually, the proteins may become entirely human with consequently little chance of eliciting a human antibody response.

D. Other Internal Emitter Therapies

The therapy provided by radioiodine for non-medullary thyroid cancer can be anticipated to continue in the indefinite future. In addition to this technique, we may anticipate other, rarer applications to increase. Among these will be the use of

MIBG (metaiodobenzylguanidine) in the treatment of neuroendocrine tumors (Shapiro et al. 1992) and the various bone pain agents described above. In the former case, diseases such as pheochromocytoma may be containable with sufficient activity levels of ^{131}I-MIBG. In the latter example, one imagines at least a continuing therapy strategy to alleviate the patient's discomfort. No other modality seems to be able to provide this service which implies a continuing increase in the number of such clinical therapies.

REFERENCES

Axelsson, B., P. Msaki, and A. Israelsson (1984). "Subtraction of Compton-scattered photons in single photon emission computed tomography." **J. Nucl. Med.** 25: 490–494.

Bayouth, J. E., D. J. Macey, A. L. Boyer, and R. E. Champlin (1995). "Radiation dose distribution within the bone marrow of patients receiving Ho-166 labeled phosphonate for marrow ablation." **Med. Phys.** 22: 743–753.

Beatty, J. D., B. G. Beatty, L. E. Williams, R. J. Paxton, J. E. Shively, M. O'Connor-Tressel (1989). "Effect of specific antibody pretreatment of liver uptake of In-111-labeled anticarcinoembryonic antigen monoclonal antibody in nude mice bearing human colon cancer xenografts." **Cancer Res.** 49: 1587–1594.

Berger, M. J. "Distribution of Absorbed Dose Around Point Sources of Electrons and Beta Particles in Water and Other Media" in **Journal of Nuclear Medicine Pamphlet No. 7.** New York: Society of Nuclear Medicine, pp. 5–23, 1971.

Berger, M. J., and S. M. Seltzer. "ETRAN, Monte Carlo Code System for Electron and Photon Transport Through Extended Media" in Oak Ridge National Laboratory Documentation for RSIC Computer Code Package CCC-107. Oak Ridge, TN: ORNL, 1973.

Bolch, W. E., L. G. Bouchet, J. S. Robertson, B. W. Wessels, J. A. Siegel, R. W. Howell, A. K. Erdi, B. Aydogan, S. Costes, and E. E. Watson (1999). "MIRD pamphlet no. 17: The dosimetry of nonuniform activity distributions—radionuclide S values at the voxel level." **J. Nucl. Med.** 40: 11S–36S.

Breitz, H. B., D. R. Fisher, P. L. Weiden, J. S. Durham, B. A. Ratliff, M. J. Bjorn, P. L. Baumier, and P. G. Abrams (1993). "Dosimetry of 186-rhenium labeled monoclonal antibodies: Methods, prediction from 99m-Tc-labeled antibodies and results of phase I trials." **J. Nucl. Med.** 34: 908–917.

Breitz, H. B., P. L. Welden, J. L. Vanderheyden, J. W. Appelbaum, M. J. Bjorn, M. F. Fer, S. B. Wolf, B. A. Ratliff, C. A. Seiler, D. C. Foisie, D. R. Fisher, R. W. Schroff, A. R. Fritzberg, and P. G. Abrams (1992). "Clinical experience with 186-rhenium labeled monoclonal antibodies for radioimmunotherapy: Results of phase I trials." **J. Nucl. Med.** 33: 1099–1112.

Briesmeister, J. (ed.). "MCNP- A General Monte Carlo N-particle Transport Code Version 4A." Los Alamos Report LA-12625. Los Alamos, NM: Los Alamos National Lab (LANL), 1993.

Brigham, E. O. **The Fast Fourier Transform.** Englewood Cliffs, NJ: Prentice-Hall, 1974.

Buras, R. R., L. E. Williams, B. G. Beatty, J. Y. C. Wong, and J. D. Beatty (1994). "A method including edge effects for the estimation of radioimmunotherapy absorbed doses in the tumor xenograft model." **Med. Phys.** 21: 287–292.

Buvat, I., M. Rodriguez-Villafuerte, A. Todd-Pokropek, H. Banali, and R. Di Paola (1995). "Comparative assessment of nine scatter correction methods based on spectral analysis using Monte Carlo simulations." **J. Nucl. Med.** 36: 1476–1488.

Chaney, E. W., and D. Kinkaid. **Numerical Mathematics and Computing.** Monterey, CA: Brooks/Cole, pp. 268–286, 1985.

Chang, L. T. (1980). "A method for attenuation correction in radionuclide computed tomography." **IEEE Trans. Nuc. Science NS** 25: 363.

D'Argenio, D. Z., and A. Schumitzky (1979). "A program package for simulation and parameter estimation in pharmacokinetic systems." **Comput. Prog. Biomed.** 9: 115–134.

deKlerk, J. M. H., A. van Dijk, A. D. van het Schip, B. A. Zonnenberg, and P. P. van Rijk (1992). "Pharmacokinetics of rhenium-186 after administration of rhenium-186-HEDP to patients with bone metastases." **J. Nucl. Med.** 33: 646–651.

DeNardo, G. L., S. J. DeNardo, L. F. O'Grady, N. B. Levy, G. P. Adams, and S. L. Mills (1990). "Fractionated radioimmunotherapy of B-cell malignancies with I-131 Lym-1." **Cancer Res.** 50 (Suppl): 1014s–1016s.

Eary, J. F., C. Collins, M. Stabin, C. Vernon, S. Petersdorf, M. Baker, S. Hartnett, S. Ferency, S. J. Addison, F. Appelbaum, and E. E. Gordon (1993). "Samarium-153-EDTMP biodistribution and dosimetry estimation." **J. Nucl. Med.** 34: 1031–1036.

Eary, J. F., O. W. Press, C. C. Badger, L. D. Durack, K. Y. Richter, S. J. Addison, K. A. Krohn, D. R. Fisher, B. A. Porter, D. L. Willliams, P. J. Martin, F. R. Appelbaum, S. L. Brown, R. A. Miller, W. B. Nelp, and I. W. Bernstein (1990). "Imaging and treatment of B-cell lymphoma." **J. Nucl. Med.** 31: 1257–1268.

Ford, R. L., and W. R. Nelson. "The EGS Code System." Stanford Linear Accelerator Report SLAC-210. Stanford, CA: Stanford University, 1978.

Foster, D. M., and R. C. Boston. "The Use of Computers in Compartmental Analysis: The SAAM and CONSAM Programs" in **Compartmental Distribution of Radiotracers.** J. S. Robertson (ed.). Boca Raton, FL: CRC Press, pp. 73–81, 1983.

Gambir, S. V., D. K. Mahoney, G. Rosenquest, M. S. Turner, and A. Wong. SIMPLE (Symbolic Interactive Modeling Package and Learning Environment). UCLA, 1991–1994.

Harbert, J. C. **Nuclear Medicine Therapy.** New York: Thieme Medical, pp. 37–89, 1987.

Howell, R. W., D. V. Rao, and K. S. R. Sastry (1989). "Macroscopic dosimetry for radioimmunotherapy: Nonuniform activity distributions in solid tumors." **Med. Phys.** 16: 66–74.

Hurley, H. R., and D. V. Becker. "The Use of Radioiodine in the Management of Thyroid Cancer" in **Nuclear Medicine Annual.** L. M. Friedman and H. S. Weiss (eds.). New York: Raven Press, pp. 329–384, 1983.

Ichihara, T., K. Ogawa, N. Motomura, A. Kubo, and S. Hashimoto (1993). "Compton scatter compensation using the triple-energy window method for single- and dual-isotope SPECT." **J. Nucl. Med.** 34: 2216–2221.

Jacobs, A. J., M. Fer, F. M. Su, H. Breitz, J. Thompson, H. Goodgold, J. Cain, J. Heap, and P. Weiden (1993). "A phase I trial of a rhenium-186-labeled monoclonal antibody administered intraperitoneally in ovarian carcinoma: toxicity and clinical response." **Obstetrics Gynecology** 82: 586–593.

Jaszczak, R. J., K. L. Greer, C. E. Floyd, C. C. Harris, and R. E. Coleman (1984). “Improved SPECT quantification using compensation for scattered photons.” **J. Nucl. Med.** 25: 893–900.

Johnson, T. K. (1988). “MABDOS: A generalized program for internal radionuclide dosimetry.” **Comput. Meth. Progr. Biomed.** 27: 159–167.

Kaplan, D. D., L. E. Williams, K. G. Clarke, T. L. Odom-Maryon, A. Liu, G. Lopatin, A. A. Raubitschek, and J. Y. C. Wong (1997). “Estimating residence times and their associated errors in patient absorbed dose calculation.” **J. Nucl. Med**. **Tech.** 25: 264–268.

Koral, K. F., F. M. Swailem, S. Buchbinder, N. H. Clinthorne, W. L. Rogers, and B. M. W. Tsui (1990). “SPECT dual-energy-window Compton correction: scatter multiplier required for quantification.” **J. Nucl. Med.** 31: 90–98.

Lewington, V. J. (1996). “Cancer therapy using bone-seeking isotopes.” **Phys. Med. Biol.** 41: 2027–2042.

Leichner, P. K. (1992). “A unified approach to photon and beta particle dosimetry.” **J. Nucl. Med.** 33: 1721–1729.

Leichner, P. K., J. L. Klein, J. B. Garrison, R. E. Jenkins, E. L. Nickoloff, D. S. Ettinger, and S. E. Order (1981). “Dosimetry of I-131 labeled anti-ferritin in hepatoma. A model for radioimmunoglobulin dosimetry.” **Int. J. Radiat. Oncol. Biol. Phys.** 7: 323–333.

Liu, A., L. E. Williams, and A. A. Raubitschek (1996). “A CT assisted method for absolute quantitation of internal radioactivity.” **Med. Phys.** 23: 1919–1928.

Liu, A., L. E. Williams, J. Y. C. Wong, and A. A. Raubitschek (1998). “Monte Carlo assisted voxel source kernel method (MAVSK) for internal beta dosimetry.” **Nucl. Med. Biol.** 25: 423–433.

Ljungberg, M., M. A. King, G. J. Hademenos, and S.-E. Strand (1994). “Comparison of four scatter correction methods using Monte Carlo simulated source distributions.” **J. Nucl. Med.** 35: 143–151.

Ljungberg, M., and S.-E. Strand (1990). “Scatter and attenuation correction in SPECT using density maps and Monte Carlo simulated scatter functions.” **J. Nucl. Med.** 31: 1560–1567.

Loevinger, R., and M. A. Berman. “A Revised Schema for Calculating the Absorbed Dose from Biologically Distributed Radionuclides” in **MIRD Pamphlet No. 1 Revised.** New York: Society of Nuclear Medicine, 1976.

Loevinger, R., E. M. Japha, and G. L. Brownell. “Discrete Radioisotope Sources” in **Radiation Dosimetry.** G. J. Hine and G. L. Brownell (eds.). New York: Academic, pp. 823–824, 1956.

Loevinger, R., T. F. Budinger, and E. E. Watson. **MIRD Primer for Absorbed Dose Calculations,** Revised Edition. New York: Society of Nuclear Medicine, 1991.

Macey, D. J., and R. Marshall (1982). “Absolute quantitation of radiotracer uptake in the lungs using a gamma camera.” **J. Nucl. Med.** 23: 731–734.

Macey, D. J., G. L. DeNardo, and S. J. DeNardo (1991). “A treatment planning program for radioimmunotherapy.” **Front. Radiat. Ther. Oncol.** 24: 123–131.

Macey, D. J., S. J. DeNardo, and G. L. DeNardo (1995). “Estimation of radiation absorbed dose for the red marrow from I-131 radiolabeled antibodies.” **Clin. Nuc. Med.** 20: 117–125.

Macey, D. J., S. J. DeNardo, G. L. DeNardo, J. L. Goodnight, and M. W. Unger (1988). “Uptake of In-111 labeled monoclonal antibody ZME018 as a function of tumor size in a patient with melanoma.” **Am. J. Physiol. Imaging** 3: 1–6.

Maksud, P., B. Fertil, C. Rica, G. El Fakhri, and A. Aurengo (1998). “Artificial neural network as a tool to compensate for scatter and attenuation in radionuclide imaging.” **J. Nucl. Med.** 39: 735–745.

McCowen, K. D., R. A. Adler, N. Ghaed, T. Verdon, and F. D. Hofeldt (1976). “Low dose radioiodide thyroid ablation in postsurgical patients with thyroid cancer.” **Am. J. Med.** 61: 52–58.

Meredith, R. F., T. K. Johnson, G. Plott, D. J. Macey, R. L. Vessella, L. A. Wilson, H. B. Breitz, and L. E. Williams (1993). “Dosimetry of solid tumors.” **Med. Phys.** 20: 583–592.

Order, S. E., J. A. Siegel, R. A. Lustig, R. Principato, L. S. Zeiger, E. Johnson, H. Zhang, P. Lang, and P. E. Waller (1994). “Infusional brachytherapy in the treatment of non-resectable pancreatic cancer: A new radiation modality (Preliminary report of the phase I study).” **Antibod. Immunoconj. Radiopharm.** 7: 11–27.

Patt, Y. Z., L. M. Lamki, T. P. Haynie, M. W. Unger, M. G. Rosenblum, A. Shirkhada, and J. L. Murray (1988). "Improved tumor localization with increasing dose of indium-111-labeled anti-carcinoembryonic antigen monoclonal antibody ZCE-025 in metastatic colorectal cancer." **J. Clin. Oncol.** 6: 1220–1230.

Press, O., J. Eary, C. C. Badger, P. J. Martin, F. R. Appelbaum, R. Levy, R. Miller, S. Brown, W. B. Nelp, K. A. Krohn, D. Fisher, K. DeSantes, B. Porter, P. Kidd, E. D. Thomas, and I. D. Bernstein (1989). "Treatment of refractory non-Hodgkin's lymphoma with radiolabeled MB-1 (Anti-CD37) antibody." **J. Clin. Oncol.** 7: 1027–1038.

Riethmuller, G., E. Schneider-Gadicke, G. Schlimok, W. Schmiegel, R. Raab, K. Hoffken, R. Gruber, H. Pichlmaier, H. Hirche, R. Pichlmayr, P. Buggisch, J. Witte (1994). "Randomised trial of monoclonal antibody for adjuvant therapy of resected Dukes'C colorectal carcinoma." **Lancet** 343: 1177–1183.

Riva, P., A. Arista, V. Tison, C. Sturiale, G. Francheschi, A. Spinelli, N. Riva, M. Casi, G. Moscatelli, and M. Frattarelli (1994). "Intralesional radioimmunotherapy of malignant gliomas: An effective treatment in recurrent tumors." **Cancer** 73 Suppl.: 1076–1082.

Roberson, P. L., D. B. Heidorn, M. L. Kessler, R. K. Ten Haken, and D. J. Buchsbaum (1994). "Three-dimensional reconstruction of monoclonal antibody uptake in tumor and calculation of beta dose-rate nonuniformity." **Cancer** 73: 912–918.

Rosenthal, M. S., J. Cullom, W. Hawkins, S. C. Moore, B. M. W. Tsui, and M. Yester (1995). "Quantitative SPECT imaging: A review and recommendations by the focus committee of the society of nuclear medicine computer and instrumentation council." **J. Nucl. Med.** 36: 1489–1513.

Samaratunga, R. C., S. R. Thomas, J. D. Hinnefeld, L. C. Von Kuster, D. M. Hyams, J. S. Moulton, M. I. Sperling, and H. R. Maxon (1995). "A Monte Carlo simulation model for radiation dose to metastatic skeletal tumor from Rhenium-186(Sn)-HEDP." **J. Nucl. Med.** 36: 336–350.

Sgouros, G. (1993). "Bone marrow dosimetry for radioimmunotherapy: theoretical considerations." **J. Nucl. Med.** 34: 689–694.

Shapiro, B., J. C. Sisson, D. M. Wieland, T. J. Mangner, S. M. Zempel, E. Mudgett, M. D. Gross, J. E. Carey, K. R. Zasadny, W. H. Beierwaltes (1992).

"Radiopharmaceutical therapy of malignant pheochromocytoma with 131-I-metaiodobenzylguanidine: Results from ten years of experience." **J. Nucl. Biol. Med.** 35: 269–276.

Shen, S., G. L. DeNardo, D. J. Macey, R. T. O'Donnell, A. Yuan, D. A. DeNardo, S. J. DeNardo (1997). "Practical determination of organ S values for individual patients for therapy." **Nucl. Med. Biol.** 24: 447–449.

Siddiqui, A. R., J. Edmondson, H. N. Wellman, R. C. Hamaker, R. E. Lingeman, H.-M. Park, and C. C. Johnston (1981). "Feasibility of low doses of 131-I for thyroid ablation in postsurgical patients with thyroid carcinoma." **Clin. Nucl. Med.** 6: 158–161.

Siegel, J. A. Thyroid Handling of Iodine-123 and Technetium-99m-pertechnetate. Ph.D. Thesis, UCLA, 1981.

Siegel, J. A., S. Whyte-Ellis, L. S. Zeigler, S. E. Order, and P. E. Walner (1994). "Bremsstrahlung SPECT imaging and volume quantitation with ^{32}Phosphorus." **Antibody Immunoconj. Radiopharm.** 7: 1–10.

Siegel, J. A., B. W. Wessels, E. E. Watson, M. G. Stabin, H. M. Vriesendorp, E. W. Bradley, C. C. Badger, A. B. Brill, C. S. Kwok, D. R. Stickney, K. F. Eckerman, D. R. Fisher, D. J. Buchsbaum, and S. E. Order (1990). "Bone marrow dosimetry and toxicity in radioimmunotherapy." **Antibod. Immunoconj. Radiopharm.** 3: 213–233.

Siegel, J. A., S. R. Thomas, J. B. Stubbs, M. G. Stabin, M. T. Hays, K. F. Koral, J. S. Robertson, R. W. Howell, B. W. Wessels, D. R. Fisher, D. A. Weber, and A. B. Brill (1999). "MIRD Pamphlet No. 16: Techniques for quantitative radiopharmaceutical biodistribution data acquisition and analysis for use in human radiation dose estimates." **J. Nucl. Med.** 40: 37S–61S.

Snyder, W. S., W. R. Ford, G. G. Warner, and S. B. Watson. "S Absorbed Dose Per Unit Cumulated Activity for Selected Radionuclides and Organs." MIRD Pamphlet No. 11. New York: Society of Nuclear Medicine, 1975.

Sorenson, J. A. "Quantitative Measurement of Radioactivity *In-Vivo* by Whole Body Counting" in **Instrumentation in Nuclear Medicine.** Vol. 2. G. J. Hine and J. A. Sorenson (eds.). New York: Academic Press, 1974.

Stabin, M. G. (1996). "MIRDOSE: Personal computer software for internal dose assessment in nuclear medicine." **J. Nucl. Med.** 37: 538–546.

Stabin, M. G., K. F. Eckerman, J. C. Ryman, and L. E. Williams (1994). "Bremsstrahlung radiation dose in yttrium-90 therapy applications." **J. Nucl. Med.** 35: 1377–1380.

Thomas, S. R., H. R. Maxon, and J. G. Kereiakes (1976). "In-vivo quantitation of lesion radioactivity using external counting methods." **Med. Phys.** 3: 253–255.

Thomas, S. R., R. H. Maxon, and J. G. Kereiakes. "Techniques for Quantitation of In Vivo Radioactivity" in **Effective Use of Computers in Nuclear Medicine.** M. J. Gelfand and S. R. Thomas (eds.). New York: McGraw-Hill, pp. 468–484, 1988.

United States Nuclear Regulatory Commission (USNRC). Release of Patients Administered Radioactive Materials. Washington D.C.: USNRC, 1997.

van Rensberg, A. J., M. G. Lotter, A. du P. Heyns, and P. C. Minnaar (1988). "An evaluation of four methods of In-111 planar image quantification." **Med. Phys.** 15: 853–861.

Wagner, J. G. **Fundamentals of Clinical Pharmacology.** Hamilton, IL: Drug Intelligence Publications Inc., pp. 231–246, 1975.

Watson, E. E., M. G. Stabin, and W. E. Bolch. Documentation Package for MIRDOSE (Version 2). Oak Ridge, TN: Oak Ridge Associated Universities, 1984.

Williams, L. E., J. Y. C. Wong, D. O. Findley, and B. W. Forell (1989). "Measurement and estimation of organ Bremsstrahlung radiation dose." **J. Nucl. Med.** 30: 1373–1377.

Williams, L. E., L. M. Ettinger, E. Cofresi, A. A. Raubitschek, and J. Y. C. Wong (1995a) "A shielded, automated injector for energetic beta-emitting radionuclides." **J. Nucl. Med. Tech.** 23: 29–32.

Williams, L. E., R. B. Bares, J. Fass, S. Hauptmann, V. Schumpelick, and U. Buell (1993). "Uptake of radiolabeled anti-CEA antibodies in human colorectal primary tumors as a function of tumor mass." **Eur. J. Nucl. Med.** 20: 345–347.

Williams, L. E., T. L. Odom-Maryon, A. Liu, A. Chai, A. A. Raubitschek, J. Y. C. Wong, and D. Z. D'Argenio (1995b). "On the correction for radioactive decay in pharmacokinetic modeling." **Med. Phys.** 22: 1619–1626.

Williams, L. E., R. B. Duda, R. T. Proffitt, B. G. Beatty, J. D. Beatty, J. Y. C. Wong, J. E. Shively, and R. J. Paxton (1988). "Tumor uptake as a function of tumor mass: A mathematic model." **J. Nucl. Med.** 29: 103–109.

Wong, J. Y. C., D. Z. J. Chu, D. Yamauchi, T. L. Odom-Maryon, L. E. Williams, A. Liu, J. M. Esteban, A. M. Wu, F. J. Primus, J. D. Beatty, J. E. Shively, and A. A. Raubitschek (1998). "Dose escalation trial of indium-111-labeled anti-carcinoembryonic antigen chimeric monoclonal antibody (cT84.66) in pre-surgical colorectal cancer patients." **J. Nucl. Med.** 39: 2097–2104.

Wu, R. K., and J. A. Siegel (1984). "Absolute quantitation of radioactivity using the buildup factor." **Med. Phys.** 11: 189–192.

Zanzonico, P. (1997). "Radiation dose to patients and families incident to I131 therapy." **Thyroidology** 7: 193–198.

APPENDIX A

Human Residence Time Estimates Made with Murine Data

The CR factor is defined in eq. (8). It is based on a relative perfusion argument. If the model animal's organ mass is the same fraction of the total body mass as is the case in the human, CR is unity. We consider a sample liver calculation using mouse biodistribution data for the antibody mT84.66.

Using the PLOT routine from MIRDOSE2, mouse liver data (in fractional injected dose per gram or FID/g) was fitted with a single exponential function. The amplitude was 0.0778/g with a $T_{1/2b}$ of 995 h. Notice that we are analyzing data corrected for the decay of the radiolabel. Using eq. (6), the effective half life became 63.56 h for an ^{111}In label. Given that value, specific murine residence time for the liver was 7.14 h/g. Since the mouse average body mass was 21.4 gram, the modified CR factor of eq. (8) became 0.56 g when a human liver was assumed to be 1833 g and a total body human mass was taken as 70 kg. Notice that we have included the animal organ mass in the uptake value so that CR is modified accordingly. Multiplying the modified CR value times the specific murine residence time of 7.14 h/g yielded a human residence time estimate of 4.00 h [τ_{liver} (human)]. Table A1 gives a summary of these results for other normal organs.

Taking this τ_{liver} value and using the MIRD Pamphlet11 table of S values resulted in a human liver-to-liver dose estimate of 0.52 rads/mCi of administered ^{111}In-labeled mT84.66 antibody. Other estimates (not shown) would follow accordingly.

Table A1. Sample Human Residence Time Estimates Made with Murine Data for ^{111}In-mT84.66

Organ	T_b	T_{ef}	FID/g	τ (mouse)/g	CR(g)	τ (human)
Blood	142 h	46 h	0.309	20.50 h	1.65	33.83 h
Liver	996	63.6	0.078	7.14	0.56	4.00
Spleen	1280	64.5	0.102	9.49	0.05	0.51
Kidneys	343	56.7	0.098	8.00	0.09	0.70
Lungs	191	50.1	0.151	10.90	0.30	3.27
Stomach	426	58.6	0.031	2.62	0.12	0.32
Bone	1429	64.8	0.033	3.09	3.05	9.42
Muscle	Infinite	67.9	0.011	1.07	9.17	9.79

APPENDIX B

Tumor Dose Estimation

Tumor FIA (fractional injected activity) was determined over a sequence of time points. Since tumor was not made part of the Figure 6 model (relatively few patients showed tumor uptake), integration of the FIA was carried out using a trapezoidal method. Size of the lesion ($5.4 \times 4.0 \times 3.0$ cm) was taken directly from the radiologist's reading of the CT scan. The resulting mass was determined with the approximation [eq. (16)] that each lateral dimension was an ellipsoidal diameter. The resultant volume was 33.9 ml or 33.9 gram if a unit density object.

For ^{90}Y, the absorbed fraction of the beta radiation for this spherical size was determined via Monte Carlo simulation as 0.91. Here, because of a lack of distribution information, uniform uptake in the metastatic site was assumed. Given the 0.43 h residence time (cf. Table C3 in Appendix C) calculated using a trapezoidal integration, the resultant dose estimate was 22.1 rad/mCi or 6.0 mGy/MBq.

APPENDIX C

Organ Data Acquired and Dose Estimates

We consider the chimeric anti-CEA antibody cT84.66 in a clinical trial (#91169). The patient (#14) had primary colon cancer with several metastatic lesions. Anterior and posterior counts were obtained at several time points using ^{111}In-cT84.66. Background was taken from an area of muscle (thigh). Table C1 contains the raw data for liver and thigh. We subtract background on the basis of counts per pixel. At 0.71 h post-injection (elapsed time), anterior and posterior images were acquired over 12 min using a dual-headed gamma camera.

Table C1. Partial List of Anterior and Posterior Counts Obtained with a Whole Body Gamma Camera

Organ	Elapsed Time (h)	Pixels	Anterior Counts	Posterior Counts
Liver (and blood)	0.71	4018	301355	254356
Soft Tissue	0.71	703	7286	6773

Using CT data, it was seen that the patient thickness (T) at the liver was 26 cm while the liver thickness (ℓ) was 16 cm. By previous attenuation measurements with an ^{111}In source, it was determined that the linear attenuation coefficient (μ) was 0.116 cm^{-1}. We subtract the background (cf. Figure 3) via:

Liver (net counts/pixel) = Liver (raw counts/pixel) – Background (counts/pixel)

For the anterior projection, this difference amounted to 64.6 counts/pixel; the posterior net count value was 53.7 counts/pixel. Upon multiplying by 4018 pixels for the liver, we obtain totals of 259×10^3 and 216×10^3 counts for anterior and posterior projections in 12 min. Their geometric mean is 237×10^3 counts in 12 minutes. The two geometric factors $\exp(\mu T/2)$ and $(\mu\ell/2)/\sinh(\mu\ell/2)$ are 4.39 and 0.869 respectively. Substituting into eq. (11) with a sensitivity of 7063×10^3 counts/(12 min IA), we obtain a fractional injected activity (FIA) of 0.128 for the liver. We should note that since this organ is imaged *in vivo*, the liver contains blood as well as hepatic tissue. Thus, the model contains both tissues for this image data.

Table C2 contains a summary of FIA for organ systems that were imaged or sampled via well counter assay. In the latter case, an aliquot of the injected dose was used to determine the FIA.

Table C2. Fractional Injected Activities (FIAs) for ^{111}In-cT84.66

Elapsed Time	Whole Body	Liver	Spleen	Heart	Tumor
0.71 h	0.993	0.128	0.027	0.168	0.0017
19.86	0.820	0.128	0.020	0.114	0.0031
42.86	0.616	0.113	0.016	0.076	0.0033
143.32	0.170	0.047	0.003	0.015	0.0010

A five-compartment model (Figure 6) was fitted to the above data set using SAAM II. The resultant residence times are given in Table C3. Notice that the model, since it contains decay as an explicit output channel from each compartment, predicts values for both ^{111}In and ^{90}Y labels on cT84.66.

Table C3. Residence Times for ^{111}In-cT84.66 and ^{90}Y-cT84.66

	Whole Body	Liver	Spleen	Heart	Red Marrow	Tumor	Residual Body
^{111}In- cT84.66	83.80 h	16.70 h	2.15 h	10.94 h	4.49 h	0.43 h	46.70 h
^{90}Y- cT84.66	80.70	15.90	2.08	10.62	4.33	0.41	45.10

We then substitute these residence times into MIRDOSE3 and obtain the values shown in Table C4.

Table C4. Estimated Absorbed Doses for cT84.66

	Whole Body	Liver	Spleen	Heart Wall	Red Marrow
^{111}In-cT84.66	0.47 rad/mCi	2.39	2.27	2.73	0.62
^{90}Y-cT84.66	2.00	16.60	22.60	24.00	4.11
^{111}In-cT84.66	0.13 mGy/MBq	0.65	0.62	0.74	0.17
^{90}Y-cT84.66	0.54	4.48	6.10	6.48	1.11

APPENDIX D

Red Marrow Data and Dose Estimation

Red marrow dose was estimated using the blood time-activity curve, measured with iv sampling, as a surrogate for the unmeasurable red marrow activity vs. time curve via eq. (20). We assumed an f factor of 0.3 in these computations with the MIRD assumptions that the plasma mass is 5.0 kg and the red marrow mass is 1.5 kg. Since we did not observe uptake in bone, we had only two source organs for ^{90}Y-cT84.66: red marrow (as represented by blood) and residual body. The corresponding residence times (4.33 h and 45.10 h) are listed in Table C3. In the case of the ^{111}In-cT84.66, all organs having measurable uptake were included as source organs.

Resulting red marrow dose estimates were then 0.62 and 4.11 rad/mCi (0.17 and 1.11 mGy/MBq) for ^{111}In-cT84.66 and ^{90}Y-cT84.66 respectively as shown in Table C4. These were based, as mentioned above, on the standard human whole blood and marrow masses. If a patient-specific red marrow dose estimate is desired, individualized mass values should be entered for these two parameters. Because of earlier therapies the red marrow mass is, however, difficult to predict for an individual RIT patient.

AAPM REPORT SERIES ($10.00 Each)

No. 1 "Phantoms for Performance Evaluation and Quality Assurance of CT Scanners" (1977)

No. 3 "Optical Radiations in Medicine: A Survey of Uses, Measurement and Sources" (1977)

No. 4 "Basic Quality Control in Diagnostic Radiology," AAPM Task Force on Quality Assurance Protocol (1977)

No. 5 "AAPM Survey of Medical Physics Training Programs," Committee on the Training of Medical Physicists (1980)

No. 6 "Scintillation Camera Acceptance Testing & Performance Evaluation," AAPM Nuclear Medicine Committee (1980)

No. 7 "Protocol for Neutron Beam Dosimetry," AAPM Task Group #18 (1980) (FREE)

No. 8 "Pulse Echo Ultrasound Imaging Systems: Performance Tests & Criteria," P. Carson & J. Zagzebski (1980)

No. 9 "Computer-Aided Scintillation Camera Acceptance Testing," AAPM Task Group of the Nuclear Medicine Committee (1982)

No. 10 "A Standard Format for Digital Image Exchange," Baxter et al. (1982)

No. 11 "A Guide to the Teaching of Clinical Radiological Physics to Residents in Radiology," AAPM Committee on the Training of Radiologists (1982)

No. 12 "Evaluation of Radiation Exposure Levels in Cine Cardiac Catherization Laboratories," AAPM Cine Task Force of the Diagnostic Radiology Committee (1984)

No. 13 "Physical Aspects of Quality Assurance in Radiation Therapy," AAPM Radiation Therapy Committee Task Group #24, with contribution by Task Group #22 (1984)

No. 14 "Performance Specifications and Acceptance Testing for X-Ray Generators and Automatic Exposure Control Devices" (1985)

No. 15 "Performance Evaluation and Quality Assurance in Digital Subtraction Angiography," AAPM Digital Radiology/ Fluorography Task Group (1985)

No. 16 "Protocol for Heavy Charged-Particle Therapy Beam Dosimetry," AAPM Task Group #20 of the Radiation Therapy Committee (1986)

No. 17 "The Physical Aspects of Total and Half Body Photon Irradiation," AAPM Task Group #29 of the Radiation Therapy Committee (1986)

No. 18 "A Primer on Low-Level Ionizing Radiation and its Biological Effects," AAPM Biological Effects Committee (1986)

No. 19 "Neutron Measurements Around High Energy X-Ray Radiotherapy Machines," AAPM Radiation Therapy Task Group #27 (1987)

No. 20 "Site Planning for Magnetic Resonance Imaging Systems," AAPM NMR Task Group #2 (1987)

No. 21 "Specification of Brachytherapy Source Strength," AAPM Radiation Therapy Task Group #32 (1987)

No. 22 "Rotation Scintillation Camera Spect Acceptance Testing and Quality Control," Task Group of Nuclear Medicine Committee (1987)

No. 23 "Total Skin Electron Therapy: Technique and Dosimetry," AAPM Radiation Therapy Task Group #30 (1988)

No. 24 "Radiotherapy Portal Imaging Quality," AAPM Radiation Therapy Task Group #28 (1988)

No. 25 "Protocols for the Radiation Safety Surveys of Diagnostic Radiological Equipment," AAPM Diagnostic X-Ray Imaging Committee Task Group #1 (1988)

No. 26 "Performance Evaluation of Hyperthermia Equipment," AAPM Hyperthermia Task Group #1 (1989)

No. 27 "Hyperthermia Treatment Planning," AAPM Hyperthermia Committee Task Group #2 (1989)

No. 28 "Quality Assurance Methods and Phantoms for Magnetic Resonance Imaging," AAPM Nuclear Magnetic Resonance Committee Task Group #1 (1990)

No. 29 "Equipment Requirements and Quality Control for Mammography," AAPM Diagnostic X-Ray Imaging Committee Task Group #7 (1990)

No. 30 "E-Mail and Academic Computer Networks," AAPM Computer Committee Task Group #1 (1990)

No. 31 "Standardized Methods for Measuring Diagnostic X-Ray Exposures," AAPM Diagnostic X-Ray Imaging Committee Task Group #8 (1991)

No. 32 "Clinical Electron-Beam Dosimetry," AAPM Radiation Therapy Committee Task Group #25 (1991)

No. 33 "Staffing Levels and Responsibilities in Diagnostic Radiology," AAPM Diagnostic X-Ray Imaging Committee Task Group #5 (1991)

No. 34 "Acceptance Testing of Magnetic Resonance Imaging Systems," AAPM Nuclear Magnetic Resonance Task Group #6 (1992)

No. 35 "Recommendations on Performance Characteristics of Diagnostic Exposure Meters," AAPM Diagnostic X-Ray Imaging Task Group #6 (1992)

No. 36 "Essentials and Guidelines for Hospital Based Medical Physics Residency Training Programs," AAPM Presidential AD Hoc Committee (1992)

No. 37 "Auger Electron Dosimetry," AAPM Nuclear Medicine Committee Task Group #6 (1993)

No. 38 "The Role of the Physicist in Radiation Oncology," Professional Information and Clinical Relations Committee Task Group #1 (1993)

No. 39 "Specification and Acceptance Testing of Computed Tomography Scanners," Diagnostic X-Ray Imaging Committee Task Group #2 (1993)

No. 40 "Radiolabeled Antibody Tumor Dosimetry," AAPM Nuclear Medicine Committee Task Group #2 (1993)

No. 41 "Remote Afterloading Technology," Remote Afterloading Technology Task Group #41 (1993)

No. 42 "The Role of the Clinical Medical Physicist in Diagnostic Radiology," Professional Information and Clinical Relations Committee Task Group #2 (1993)

No. 43 "Quality Assessment and Improvement of Dose Response Models," $25, (1993).

No. 44 "Academic Program for Master of Science Degree in Medical Physics," AAPM Education and Training of Medical Physicists Committee (1993)

No. 45 "Management of Radiation Oncology Patients with Implanted Cardiac Pacemakers," AAPM Task Group #4 (1994)

No. 46 "Comprehensive QA for Radiation Oncology," AAPM Radiation Therapy Committee Task Group #40 (1994)

No. 47 "AAPM Code of Practice for Radiotherapy Accelerators," AAPM Radiation Therapy Task Group #45 (1994)

No. 48 "The Calibration and Use of Plane-Parallel Ionization Chambers for Dosimetry of Electron Beams," AAPM Radiation Therapy Committee Task Group #39 (1994)

No. 49 "Dosimetry of Auger-Electron-Emitting Radionuclides," AAPM Nuclear Medicine Task Group #6 (1995)

No. 50 "Fetal Dose from Radiotherapy with Photon Beams," AAPM Radiation Therapy Committee Task Group #36 (1995)

No. 51 "Dosimetry of Interstitial Brachytherapy Sources," AAPM Radiation Therapy Committee Task Group #43 (1995)

No. 52 "Quantitation of SPECT Performance," AAPM Nuclear Medicine Committee Task Group #4 (1995)

No. 53 "Radiation Information for Hospital Personnel," AAPM Radiation Safety Committee (1995)

No. 54 "Stereotactic Radiosurgery," AAPM Radiation Therapy Committee Task Group #42 (1995)

No. 55 "Radiation Treatment Planning Dosimetry Verification," AAPM Radiation Therapy Committee Task Group #23 (1995), $48, (Includes 2 disks, ASCII format). Mail, fax, or phone orders to: AAPM Headquarters, One Physics Ellipse, College Park, MD 20740-3846, Phone: (301) 209-3350, Fax: (301) 209-0862

No. 56 "Medical Accelerator Safety Considerations," AAPM Radiation Therapy Committee Task Group #35, Reprinted from *Medical Physics*, Vol. 20, Issue 4, July/August 1993

No. 57 "Recommended Nomenclature for Physical Quantities in Medical Applications of Light," AAPM General Medical Physics Committee Task Group #2 (1996)

No. 58 "Managing the Use of Fluoroscopy in Medical Institutions," AAPM Radiation Protection Committee Task Group #6 (1998)

No. 59 "Code of Practice for Brachytherapy Physics," AAPM Radiation Therapy Committee Task Group #56, Reprinted from *Medical Physics*, Vol. 24, Issue 10, October 1997

No. 60 "Instrumentation Requirements of Diagnostic Radiological Physicists," AAPM Diagnostic X-Ray Committee Task Group #4 (1998)

No. 61 "High Dose Brachytherapy Treatment Delivery," AAPM Radiation Therapy Committee Task Group #59, Reprinted from *Medical Physics*, Vol. 25, Issue 4, April 1998

No. 62 "Quality Assurance for Clinical Radiotherapy Treatment Planning," AAPM Radiation Therapy Committee Task Group #53, Reprinted from *Medical Physics*, Vol. 25, Issue 10, October 1998

No. 63 "Radiochromic Film Dosimetry," AAPM Radiation Therapy Committee Task Group #55, Reprinted from *Medical Physics*, Vol. 25, Issue 11, November 1998

No. 64 "A Guide to the Teaching of Clinical Radiological Physics To Residents in Diagnostic and Therapeutic Radiology," Revision of AAPM Report #11, AAPM Committee on the Training of Radiologists, January 1999

No. 65 "Real-Time B-Mode Ultrasound Quality Control Test Procedures," AAPM Ultrasound Task Group #1, Reprinted from *Medical Physics*, Vol. 25, Issue 8, August 1998

No. 66 "Intravascular Brachytherapy Physics," AAPM Radiation Therapy Committee Task Group #60, Reprinted from *Medical Physics*, Vol. 26, Issue 2, February 1999

No. 67 "Protocol for Clinical Reference Dosimetry of High-Energy Photon and Electron Beams," AAPM Task Group #51, Reprinted from *Medical Physics*, Vol. 26, Issue 9, September 1999

No. 68 "Permanent Prostate Seed Implant Brachytherapy," AAPM Medicine Task Group #64, Reprinted from *Medical Physics*, Vol. 26, Issue 10, October 1999

No. 69 "Recommendations of the AAPM on ^{103}Pd Interstitial Source Calibration and Dosimetry: Implications for Dose Specification and Prescription," Report of the Low Energy Interstitial Brachytherapy Dosimetry Subcommittee of the Radiation Therapy Committee, In progress (2001)

No. 70 "Cardiac Catherization Equipment Performance," Task Group #17 Diagnostic X-ray Imaging Committee, February 2001

No. 71 "A Primer for Radioimmunotherapy and Radionuclide Therapy," Task Group #7 Nuclear Medicine Committee, April 2001

Return to: Medical Physics Publishing
4513 Vernon Blvd.
Madison, WI 53705-4964
(800) 442-5778 phone
(608) 265-2121 FAX

Name: _____

Address: _____

_____

_____ copies of_____ @_____

_____ copies of_____ @_____

_____ copies of_____ @_____

Prepayment required
U.S. check or International Money Order

Amount enclosed $_____